

## LETTERS IN BIOMATHEMATICS An International Journal



#### RESEARCH ARTICLE

**3** OPEN ACCESS

# Modeling Seasonal Malaria Transmission: A Methodology Connecting Regional Temperatures to Mosquito and Parasite Developmental Traits

Olivia Prosper<sup>a</sup>, Katharine Gurski<sup>b</sup>, Miranda I. Teboh-Ewungkem<sup>c</sup>, Angela Peace<sup>d</sup>, Zhilan Feng<sup>e</sup>, Margaret Reynolds<sup>f</sup>, Carrie Manore<sup>g</sup>

- <sup>a</sup> Department of Mathematics, University of Tennessee Knoxville; <sup>b</sup>Department of Mathematics, Howard University;
- <sup>c</sup>Department of Mathematics, Lehigh University; <sup>d</sup>Department of Mathematics and Statistics, Texas Tech University;
- <sup>e</sup>Department of Mathematics, Purdue University; <sup>f</sup>Department of Mathematical Sciences, West Point; <sup>g</sup>Information Systems and Modeling, Los Alamos National Laboratory

#### **ABSTRACT**

Increasing temperatures have raised concerns over the potential effect on disease spread. Temperature is a well known factor affecting mosquito population dynamics and the development rate of the malaria parasite within the mosquito, and consequently, malaria transmission. A sinusoidal wave is commonly used to incorporate temperature effects in malaria models, however, we introduce a seasonal malaria framework that links data on temperature-dependent mosquito and parasite demographic traits to average monthly regional temperature data, without forcing a sinusoidal fit to the data. We introduce a spline methodology that maps temperature-dependent mosquito traits to time-varying model parameters. The resulting non-autonomous system of differential equations is used to study the impact of seasonality on malaria transmission dynamics and burden in a high and low malaria transmission region in Malawi. We present numerical simulations illustrating how temperature shifts alter the entomological inoculation rate and the number of malaria infections in these regions.

#### **ARTICLE HISTORY**

Received May 25, 2022 Accepted November 23, 2022

#### **KEYWORDS**

malaria, seasonal, temperature-dependent, non-autonomous, cubic splines, data

## 1 Introduction

Malaria continues to be a burden in many parts of the world even though there have been appreciable reductions in morbidity and mortality in the last two decades. These reductions are attributable to vector-targeted control measures—including the use of insecticide-treated nets (ITNs), indoor residual spraying (IRS), larvicides, mosquitocidal drugs such as ivermectin and more (Teboh-Ewungkem and Ngwa, 2020; Slater et al., 2020; Ngwa et al., 2019)—and human-targeted control measures—including the use of Intermittent Preventive Treatment (IPT) as a control tool or the ITNs, as a human-mosquito contact reduction measure (WHO, 2021a,b; Teboh-Ewungkem et al., 2015, 2014; Manore et al., 2019)—to name a few. However, the World Health Organization (WHO) estimated that there were 229 million malaria cases resulting in a little over 400,000 deaths in 2019, with 67% of those deaths (approx. 270,000) occurring in children under the age of five (WHO, 2021a). The recent December 2021 WHO malaria statistic is even more concerning as there was an uptick in malaria cases and deaths in 2020: an estimated 241 million cases resulting in about 627,000 deaths in 2020, with an estimated 80% of those deaths occurring in children under five (WHO, 2021a). Some of the recent increase in the malaria deaths may be attributed to disruptions in malaria interventions as a consequence of the COVID-19 pandemic (Weiss et al., 2020; Teboh-Ewungkem and Ngwa, 2021). With the continuous initiative aimed at zeroing in on malaria elimination, it is important to continue to understand and investigate all facets of the challenges that exist as it relates to a successful malaria control/elimination program.

One such challenge involves changes in temperatures that have been observed over the recent year, with temperature a well known factor affecting mosquito population dynamics and malaria transmission disease dynamics (Johnson and Riess, 1982; Beck-Johnson et al., 2013), as shown in Figure 1. We note that mosquito population dynamics and malaria parasite development has a nonlinear relationship to temperature, as shown in (Baton and Ranford-Cartwright, 2005; Suh et al., 2020; Pathak

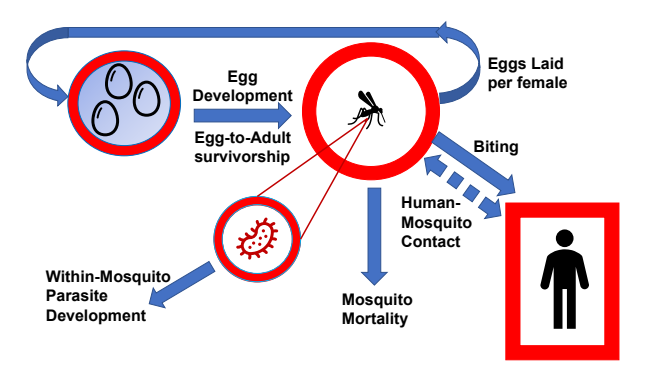


**Figure 1:** Schematics showing mosquito- and human-linked parameters affected by temperature. These parameters are those linked to mosquito growth and survivability, and those linked to disease transmission. The parameters linked to mosquito growth and survivability are: the mosquito biting/feeding rate, egg development rate, mosquito mortality rate, and growth from larva to adult mosquito, while those linked to disease transmission are the within-mosquito parasite development rate as well as the human-mosquito contact rates, associated to the biting rate.

et al., 2019; Dawes et al., 2009; Teboh-Ewungkem et al., 2010; Teboh-Ewungkem and Yuster, 2010; Mordecai et al., 2019) thus emphasizing the need to to understand wide temperature swings (increase and decrease) that accompany climatic change.

Pascual et al. (2006) noted that the impact of temperature on mosquito dynamics can dramatically amplify mosquito abundance, and therefore, potentially disease transmission. Consequently, even small increases in temperature could have important implications for malaria transmission. An understanding of the temperature effects warrants a brief discussion of the malaria transmission dynamics. The malaria parasite, the responsible pathogen that causes malaria, is transmitted from one human to another by adult female Anopheles mosquitoes. Thus, the parasite lives part of its life cycle in the mosquito and part in the human. Hence, the size of the adult *Anopheles* mosquito population at any given time, as well as the size of the aquatic progenitor stages, are important factors to consider when determining malaria disease risk and burden in a region. Temperature plays a significant role in the developmental aquatic life stages of the Anopheles mosquito, as well as their survivability (Baton and Ranford-Cartwright, 2005). Moreover, high temperatures affect the development of the within-mosquito parasite forms, and hence the extrinsic incubation period of the parasite (i.e., the time between ingestion of male and female gametocytes by an infectious mosquito to when the mosquito is infectious) (Baton and Ranford-Cartwright, 2005; Suh et al., 2020; Pathak et al., 2019; Dawes et al., 2009; Teboh-Ewungkem et al., 2010; Teboh-Ewungkem and Yuster, 2010; Mordecai et al., 2019). In particular, in their laboratory experimental results, Suh et al. (2020) observed that thermal sensitivity of malaria parasites during the initial stages of parasite development within the mosquito impacted mosquito competence (i.e., its ability to become infected, allow replication, and become infectious). Pathak et al. (2019) studied A. stephensi at three mean temperatures of 20-28°C with a 9°C daily gradient ( $-4^{\circ}$ C to +5°C of mean). Their results showed that for the same gametocyte densities at 28°C there was a severe reduction in sporozoite rates leading to a decline in vector competence as compared to sporozoite rates at 24°C. Earlier, Dawes et al. (2009) found that A. stephensi mortality is dependent on the age of mosquito and the density of the Plasmodium infection. A summary of thermal optima and limits across vector-borne diseases is given by Mordecai et al. (2019). For P. falciparum malaria, results include a thermal optima at (25–26°C) for the A. gambiae, A. spp, and A. stephensi.

Another challenge is the high variability in transmission across regions, with some regions experiencing stable malaria transmission year-round, and others experiencing intense intervals of seasonal transmission, corresponding to one or two wet seasons each year. This means that a one-program-fits-all global control is not ideal, but rather a region-based control effort is needed for effective disease management. Such a control effort should consider temperature effects on mosquito abundance, which inadvertently would impact malaria transmission, as well as temperature effects on parasite development within a mosquito host. Hence, studying seasonality under these varied temperature conditions is essential.

Other authors have studied the effects of seasonal temperature on malaria dynamics. For example, Agusto et al. (2015) and Agusto (2020) used the mosquito and parasite temperature data from Mordecai et al. (2013) but with a yearly sinusoidal temperature variation, which differs from the methodology being proposed here. Here, we utilize regional recorded average monthly temperature data. Garba and Danbaba (2020) presented a model that accounted for temperature effects on certain parameters (aquatic and adult mosquito per capita death rates, mosquito oviposition, maturation and survival, as well as biting rates) associated with mosquito growth potential. These parameters were defined by either Briere or quadratic functions, as mostly defined by Mordecai et al. (2013). They used their model to assess the effects of changes in temperatures on some set of control strategies, including one related to the use of bednets. However, in their simulation, they used a generalized sinusoidal temperature function. This work was similar to earlier work by Okuneye and Gumel (2017), in which they proposed a model that

accounted for age-structure in the human population as well as aquatic mosquito dynamics. Using this model, they investigated the effects of temperature and rainfall on malaria transmission in Kwazulu Natal. They reported that in the studied region, transmission was maximized when the mean monthly temperature, irrespective of rainfall, fell in the range between 21 and 25 degrees Celsius and rainfall was between 95 and 125 mm. We note that the work of Garba and Danbaba (2020) and of Okuneye and Gumel (2017) only considered mosquito-related temperature effects; temperature effects on parasite dynamics were not considered. Artzy-Randrup et al. (2010) demonstrated through mathematical modeling of malaria and immunity that temperature can influence the spread of drug resistance via its impact on disease transmission. In particular, they identified two thresholds, one for which an increase in temperature decreases drug resistance, and a second that allows drug resistance to reestablish itself. This modeling along with time series data, helped to explain the increase in the spread of drug resistant malaria in Kenya under the influence of warming temperatures. Further discussions on historical perspectives on mathematical models in relation to climatic factors can be found in the comprehensive review of Eikenberry and Gumel (2018) and the references therein.

In this manuscript, we propose a malaria transmission model in which temperature effects are considered for both the malaria transmitting mosquitoes and the malaria causing parasite. Using local temperature data, we create seasonal profiles unique to a malaria transmission locality based on average monthly temperature data, without forcing a sinusoidal fit to the data. We do so by introducing a continuous spline function that maps temperature-dependent mosquito and parasite traits to time-dependent parameters. The resulting temperature-to-time converted data is then embedded into our mathematical model and used to study the impact of seasonality on malaria burden and transmission dynamics in two selected malaria regions in Malawi, Africa, over a short-term period. Malawi, a country in sub-saharan Africa, has been identified as a region particularly vulnerable to the impacts of climate change: the prevalence of poverty, diseases like malaria, HIV/AIDS, and diarrhea, and the strong reliance on agriculture within the country for both food and income, makes this country highly vulnerable to changes in temperature and rainfall (Warnatzsch and Reay, 2019). Temperature data for Malawi from 1961 to 2005 indicates an annual rate of temperature increase of 0.3°C per year (Warnatzsch and Reay, 2019). Kavwenje et al. (2022) projected an increase in the mean seasonal maximum temperature in Malawi of 1.63 to 2.48 degrees celsius in the 2050s, and between 2.32 and 4.68 degrees celsius in the 2080s. Likewise, the mean seasonal minimum temperature is projected to increase by 1.74–2.53 in the 2050s and 2.41– 4.60 in the 2080s. While there is variation in the magnitude of the increase between seasons, they projected that temperatures would increase across all seasons. Although the majority of climate models considered by Kavwenje et al. (2022) consistently projected temperature increases in this region, one model did suggest the possibility of a temperature decrease. With the idea that climate change can lead to more extreme weather, we considered the impact of both increases and decreases in monthly temperature in this study. Furthermore, an increase in elevation of 1000 m coincides with a roughly 6 degree C decrease in temperature, so considering negative temperature shifts allows us to explore what we may expect to see in neighboring regions with higher elevation (Pascual et al., 2006). Additionally, Malawi has a history of drug resistance to Chloroquine. After ceasing the use of this monotherapy, Chloroquine efficacy eventually re-emerged. It is thought that this result is in part due to areas of lower transmission in regions of Malawi, in which drug resistant genes are less likely to become fixed. Studies monitoring drug resistance in pregnant women undergoing ITPp (Intermittent Preventive Treatment in pregnant women) indicate an increase in drug-resistant mutations in these individuals. Consequently, monitoring the spread of drug resistance in Malawi is a public health concern, which may be amplified by a warming climate. As a result, we include both drug resistant and drug sensitive strains of malaria in our mathematical model (Plowe, 2022).

The selected regions where we apply our methodology are the Blantyre district, a low malaria transmission region, and the Chikwawa district, a high malaria transmission region, both located in Southern Malawi, and with malaria infections largely attributed to P. falciparum (Coalson et al., 2016). Our aim is to demonstrate the effect that fluctuating seasonal temperatures, as well as shifts in seasonal temperatures within the range [-2, +2] degrees Celsius, have on malaria transmission and burden in a high transmission and a low transmission region. We also compute the time-dependent threshold (reproduction) and invasion numbers, monthly Entomological Inoculation Rates (mEIR), and investigate possible co-existence between a drug-sensitive malaria strain and a drug-resistant malaria strain within the temperature range noted, assessing malaria disease risks in relation to temperature shifts.

The use of Spline methodology to incorporate temperature data into biological models is not entirely new. For example, Sippy et al. (2019) examined the effect of climate on dengue in Ecuador, finding that dengue diagnoses peak once per year in mid-March and were impacted by regional climate and complex interactions between local weather variables. The model found that the most important predictors of dengue fever were annual sinusoidal fluctuations in disease and long-term trends which were represented by a spline for the full study duration. Adegboye et al. (2019) fit data from three major leishmaniasis-afflicted provinces of Afghanistan between 2003 and 2009 to non-linear and distributed lag non-linear models by applying a spline function to describe the time dependency along the range of values with a lag of up to 12 months. Then Kindong et al. (2021) incorporated four generalized additive models, each comprising different spline terms, to analyze the influence of the measured variables on the abundance of two fish species in the Yangtze river estuary with three years of environmental variables. While the use of Spline methodology in biological models is not entirely new, its use on malaria models as proposed here appears novel



in that temperature effects for malaria specific regions can be accounted for and compared. With this method we can combine biological data for mosquitoes and malaria parasites with temperatures of specific regions and then use the modeling results to illustrate the impact of seasonality on malaria as well as on spread of drug resistance (using, for example, time-dependent reproduction and invasion numbers). Thus our results can serve to inform region specific control and policies.

Our mathematical model, the data, and parameterization of the seasonal mosquito attributes are described in Section 2. In Section 3 we present the derivation for the strain-specific reproduction numbers for the perennial and seasonal transmission models. We also derive the periodic invasion threshold numbers for the resistant strain. In Section 4, we present results for the numerical simulations of the model. Finally, we interpret these results in Section 5 and conclude with our overarching message and future work.

#### 2 Models & Methods

### 2.1 Model without seasonality

Here, we use a modification of the model originally proposed in (Teboh-Ewungkem et al., 2015) without the incorporation of Intermittent Preventive Treatment (IPT), to model malaria transmission dynamics in a population under the spread of both resistant and sensitive parasite strains. The model, a compartmental differential equation model, describes the dynamics of the population changes in seven human compartments and three mosquito compartments distinguished by their parasite status and treatment status for the case of humans. At any time t, the human compartments are: susceptible humans (individuals with no parasites in their blood stream) modeled by S; infected/infectious humans infected with the sensitive parasite strain, modeled by  $I_s$  if symptomatic, or  $I_a$  if asymptomatic; infected/infectious humans infected with the resistant parasite strain and modeled by  $I_s$  if symptomatic or  $I_a$  if asymptomatic; treated symptomatic humans modeled by  $I_s$  and recovered humans modeled by  $I_s$ . The mosquito compartments are described using the variables  $S_v$ , which represents the population of mosquitoes with no parasites in them;  $M_s$ , which represents the population of mosquitoes infected with the sensitive parasite strain and  $M_r$ , those mosquitoes infected with the resistant parasite strain.

The model assumes that movement from the susceptible human class to an infected/infectious class is as a result of a bite from an infectious mosquito. If the bites are from mosquitoes infected with the sensitive parasite strain, then a fraction  $\lambda_I$  of these humans would progress with symptoms to the symptomatic infected/infectious class  $(I_s)$ , while the remaining fraction progresses to the asymptomatic class  $(I_a)$ . Likewise, if the bites are from mosquitoes infected with the resistant parasite strain, then a fraction  $\lambda_I$  of these humans will progress with symptoms to the symptomatic infected/infectious class  $(I_s)$ , with the remaining fraction progressing to the asymptomatic class  $(I_a)$ . The sizes of these proportions  $\lambda_I$ ,  $\lambda_I$ , whether close to one or zero would depend on whether the region is characterized as high or low transmission. High transmission regions are more likely to have high rates of asymptomatic infections as a result of repeated exposure to malaria and the gradual development of naturally acquired immunity. We note that this is an updated assumption from the model in (Teboh-Ewungkem et al., 2015) were we had assumed  $\lambda_I = \lambda_I$ .

Symptomatic infected individuals infected with the sensitive strain can clear their infection via treatment at rate  $ap_I$  by taking a WHO recommended drug, where 1/a days is the average time from drug administration to when the administered drug levels are high enough to clear drug-sensitive parasite strains (i.e., the therapeutic level). As in (Teboh-Ewungkem et al., 2015),  $p_I \in (0,1]$  is the drug treatment efficacy of a sensitive parasite strain; a value less than 1 depicts a situation where an individual does not take the full WHO-recommended therapeutic dose for the required length of time or takes a fake drug. A symptomatic infected individual infected with the resistant strain can clear their infection via treatment at rate  $ap_I$ , where a is as described earlier and  $p_I \in [0, 0.5)$  is the drug treatment efficacy of a drug-resistant parasite strain;  $p_I = 0$  depicts the scenario of full resistance with the drug totally refractory to treatment. We do assume and will expect that when the drug under consideration is the WHO recommended drug with the right dose taken for the required length of time, we will have  $p_I \ll p_I = 1$ . Symptomatic infected individuals who do not seek treatment can also clear their infection naturally at rate  $\sigma_s$ . However, we assume that fraction  $\xi_L$  of these individuals infected with the sensitive strain who naturally clear their infection will develop temporary immunity. Similarly, we assume that fraction  $\xi_L$  of those individuals infected with the resistant strain who naturally clear their infection will develop temporary immunity. The remaining fractions join the susceptible class. We additionally assume that resistant infections may have a reduced natural clearance rate and hence for resistant infections, we scale  $\sigma_s$  by  $\phi \in (0,1]$ . We note that we do not consider IPT in this study and instead focus on the treatment of infected individuals using a parameterization suitable for the short half-life antimalarial drug chlorproguanil-dapsone (CPG-DDS), consistent with our previous studies (Teboh-Ewungkem et al., 2015; Manore et al., 2019; Teboh-Ewungkem et al., 2014).

On the other hand, we assume that asymptomatic infectious individuals do not seek treatment and can only clear their infections naturally, at rate  $\sigma_a$ . Of these asymptomatic infections, fractions  $\xi_{I_a}$  naturally clear their sensitive infections and  $\xi_{I_a}$  naturally clear their resistant infections, developing temporary immunity, while the remaining fractions rejoin the susceptible class. Similar to the discussion in the preceding paragraph, we assume that resistant infections may have a reduced natural clearance rate



and hence for resistant infections we scale  $\sigma_a$  by  $\phi \in (0, 1]$ . We also assume that asymptomatic infectious individuals can develop symptoms at rate  $\nu$  and join the  $I_s$  or  $J_s$  classes based on their parasite strain. Additionally, we assumed cross-immunity between sensitive and resistant strains, so that when individuals recover naturally from drug-sensitive or drug-resistant infections, they progress to the same recovered class.

Treated individuals are protected against the sensitive strain, but remain susceptible to the resistant strain at a reduced rate, where  $\zeta$  represents the scale factor that reduces the transmissibility of the parasite to treated humans. Treatment may interrupt the development of immunity for some individuals, hence a proportion of treated individuals return to susceptible once they've cleared the drug from their system. Finally, we assume constant recruitment into the susceptible human class at rate  $\Lambda_b$  and into the susceptible mosquito class  $\Lambda_v$  (non-constant in the seasonal model), and assume natural death rates  $\mu_b$  and  $\mu_v$  (non-constant in the seasonal model) from all human and mosquito classes respectively.

As previously mentioned, our model here is based on the model presented in (Teboh-Ewungkem et al., 2015) with some key differences. We do not consider IPT, but allow for the possibility of development of different levels of temporal immune responses following natural clearance of the parasite. These levels are captured by the proportions of symptomatic infections,  $\xi_{I_a}$  and  $\xi_{J_a}$ , asymptomatic infections,  $\xi_{I_a}$  and  $\xi_{J_a}$ , and treated infections,  $\xi_{T_i}$ , all cleared naturally leading to the development of temporary immunity. These parameter values in essence capture different heterogeneous regions. Additionally, in the analysis of (Teboh-Ewungkem et al., 2015), the base value for the scale factor that reduces the rate of natural clearance of resistant parasites relative to sensitive parasites,  $\phi$ , was 1.

Putting all these model assumptions together yields the following equations for the human compartments:

$$\frac{dS}{dt} = \Lambda_b - \beta_b (M_s + \kappa_b M_r) S / N_b + \sigma_a ((1 - \xi_{I_a}) I_a + (1 - \xi_{J_a}) \phi J_a) 
+ \sigma_s ((1 - \xi_{I_s}) I_s + (1 - \xi_{J_s}) \phi J_s) + (1 - \xi_{T_s}) r_s T_s + \omega R - \mu_b S,$$
(1a)

$$\frac{dI_s}{dt} = \lambda_I \beta_b M_s S / N_b + \nu I_a - (a p_I + \sigma_s + \mu_b + \delta) I_s, \tag{1b}$$

$$\frac{dI_a}{dt} = (1 - \lambda_I)\beta_b M_s S/N_b - (\nu + \sigma_a + \mu_b)I_a, \tag{1c}$$

$$\frac{dJ_s}{dt} = \lambda_J \kappa_{bl} \beta_b M_r (S + \zeta T_s) / N_b + \nu J_a - (ap_J + \phi \sigma_s + \mu_b + \delta) J_s, \tag{1d}$$

$$\frac{dJ_a}{dt} = (1 - \lambda_J)\kappa_b\beta_b M_r (S + \zeta T_s)/N_b - (\phi\sigma_a + \nu + \mu_b)J_a, \tag{1e}$$

$$\frac{dT_s}{dt} = ap_I I_s + ap_J J_s - r_s T_s - \zeta \kappa_b \beta_b M_r T_s / N_b - \mu_b T_s, \tag{1f}$$

$$\frac{dR}{dt} = \sigma_s(\xi_{I_s}I_s + \xi_{J_s}\phi J_s) + \sigma_a(\xi_{I_a}I_a + \phi \xi_{J_a}J_a) + \xi_{T_s}r_sT_s - (\omega + \mu_b)R. \tag{1g}$$

The total human population is  $N_b = S + I_s + I_a + J_s + J_a + T_s + R$ , which is modeled by the equation

$$\frac{dN_b}{dt} = \Lambda_b - \mu_b N_b - \delta(I_s + J_s). \tag{2}$$

The total human population has a disease-free carrying capacity of  $N_b^* = \Lambda_b/\mu_b$ . The equations that govern the mosquito dynamics are

$$\frac{dS_v}{dt} = \Lambda_v - \beta_v \left[ I_a + I_s + \kappa_v (J_a + J_s) \right] S_v / N_b - \mu_v S_v, \tag{3a}$$

$$\frac{dM_s}{dt} = \beta_v (I_a + I_s) S_v / N_h - \mu_v M_s, \tag{3b}$$

$$\frac{dM_r}{dt} = \kappa_v \beta_v (J_a + J_s) S_v / N_b - \mu_v M_r, \tag{3c}$$

where the total mosquito population is  $N_v = S_v + M_s + M_r$  and is modeled by the equation

$$\frac{dN_v}{dt} = \Lambda_v - \mu_v N_v. \tag{4}$$

A flow diagram for the human transmission dynamics of the model is given in Figure 2, while that for the mosquito transmission dynamic is given in Figure 3. Table 1 gives a summary of the state variable descriptions, while Tables 2 and 3 give the parameter descriptions. All the variables and parameters are non-negative. Additionally, in Figure 1, we show the temperature-dependent components of the model.

Table 4 contains the parameter values that are unchanged across high and low transmission scenarios while Table 5 contains the parameter values that vary across high and low transmission regions.

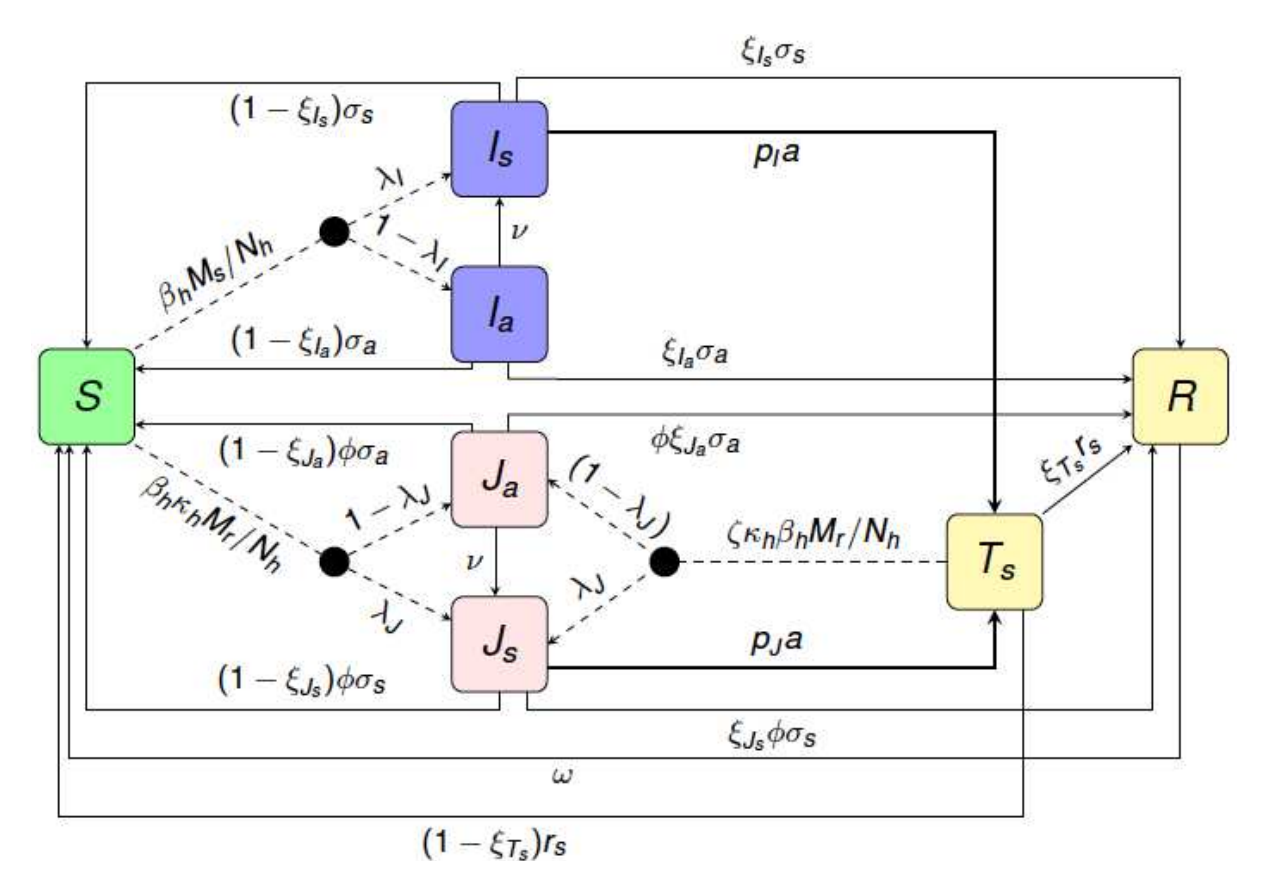


**Figure 2:** Transfer diagram for human infection transmission dynamics. Dashed lines represent parasite transmission via infected mosquitoes; thick solid lines represent treatment of symptomatic infected individuals; thin solid lines represent either recovery or progression from asymptomatic to symptomatic infection. I (in blue) infections are with sensitive strains and J (in red) with resistant strains of malaria with subscripts a and s representing asymptomatic and symptomatic cases.  $T_s$  is individuals receiving effective treatment for a symptomatic case. S (in green) is fully susceptible and R is temporarily immune.

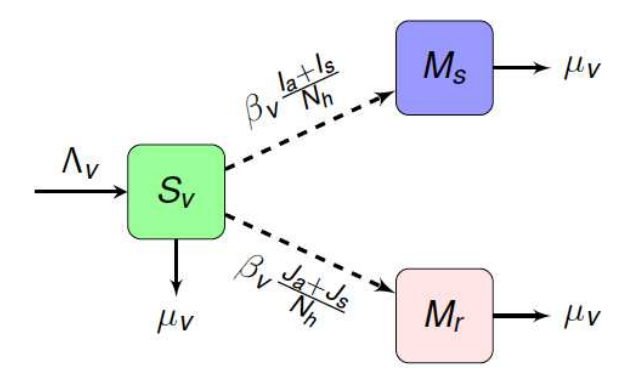


**Figure 3**: Transfer diagram for mosquito infection transmission dynamics. Dashed lines represent parasite transmission via mosquito biting infected humans.  $M_s$  (in blue) infections are with sensitive strains and  $M_r$  (in red) with resistant strains of malaria parasites  $S_v$  (in green) is fully susceptible mosquitos.

**Table 1**: State variables and their descriptions.

Variable	Description			
$S_v$	Number of susceptible mosquitoes			
$M_{\scriptscriptstyle S}$	Number of mosquitoes infected with the sensitive parasite strain			
$M_r$	Number of mosquitoes infected with the resistant malaria parasite strain			
S	Number of susceptible humans			
$I_{\scriptscriptstyle \mathcal{S}}$	Number of symptomatic infected humans infected with the sensitive malaria parasite strain			
$I_a$	Number of asymptomatic infected humans infected with the sensitive malaria parasite strain			
$J_s$	Number of symptomatic infected humans infected with the resistant malaria parasite strain			
$J_a$	Number of asymptomatic infected humans infected with the resistant malaria parasite strain			
$T_s$	Number of symptomatic infected humans who are treated			
R	Number of infected humans who clear their parasite either naturally or			
	via treatment and develop temporary immunity			
$N_{b}$	Total human population			
$N_v$	Total mosquito population			

**Table 2:** Descriptions and dimensions for parameters related to the natural transmission cycle. We let H be the quasi-dimension for humans, M the quasi-dimension for mosquitoes, T for time, and B for bites. Note that  $\Lambda_v$ ,  $\mu_v$ ,  $\beta_v$ , and  $\beta_h$  are functions in seasonal model.

Parameter	r Description			
$\Lambda_b$	Recruitment rate into the human population			
$\Lambda_v$	Recruitment rate into the mosquito population			
$\mu_b$	Per capita death rate of humans			
8	Malaria disease-induced mortality rate for humans			
$\mu_v$	Natural mosquito death rate	$T^{-1}$		
$\beta_{b}$	Transmission rate of sen. parasites from mosquitoes to humans	H/(MT)		
$eta_v$	Transmission rate of sen. parasites from humans to mosquitoes	$T^{-1}$		
$\kappa_{h}$	Reduction factor of human transmission rate by the resistant parasite strain			
$\kappa_v$	Reduction factor of mosquito transmission rate by the resistant parasite strain			
$\lambda_I$	Fraction of humans who become symptomatic following infection with the sensitive malaria parasite strain			
$\lambda_J$	Fraction of humans who become symptomatic following infection with the resistant malaria parasite strain			
$\omega$	Rate of loss of temporary immunity in humans	$T^{-1}$		
ν	Rate at which humans progress from asymptomatic to symptomatic infections	$T^{-1}$		
$\sigma_a$	Rate of naturally clearing an asymptomatic infection for humans	$T^{-1}$		
$\sigma_{s}$	Rate of naturally clearing a symptomatic infection for humans	$T^{-1}$		
$\phi$	Scale factor that reduces the rate of natural clearance of resistant parasites relative to sensitive parasites			
ζ	Scale factor that reduces transmissibility of the parasite to treated humans			
$\xi_{I_s},\ \xi_{J_s}$	Proportion of symptomatic humans who naturally clear their infection and develop temporary immunity			
$\xi_{I_a},\ \xi_{J_a}$	Proportion of asymptomatic humans who naturally clear their infection and develop temporary immunity			
$\xi_{T_s}$	Proportion of treated humans who after clearance of their infection develop temporary immunity			
m	Ratio of mosquitoes to humans	$MH^{-1}$		
α	Per-mosquito biting rate	$BM^{-1}T^{-1}$		
$eta_{vh}$	Number of mosquitoes that get infected given a bite on an infected host	$MB^{-1}$		
$eta_{hv}$	Number of susceptible humans that get infected given a bite from an infected mosquito	$HB^{-1}$		



Table 3: Descriptions and dimensions for parameters related to symptomatic treatment for a given drug

Parameter	Description	Dimension
1/a	Days to clear a sensitive infection after treatment	T
$1/r_s$	Time chemoprophylaxis lasts in symptomatic treated humans	T
$p_I$	Efficacy of drugs used to clear sensitive infections	
ÞЈ	Efficacy of drugs used to clear resistant infections	

**Table 4:** Parameter values, ranges, and references that are unchanged across high/low transmission scenarios.

Parameter	Value Range	Baseline	Reference
$N_b(0)$		5 × 10 <sup>6</sup>	Manore et al., 2019
$N_v(0)$		$mN_h(0)$	assumed
$\Lambda_{b}$	$(2.24 \times 10^3, 5.08 \times 10^3)$	$3.55 \times 10^{3}$	Manore et al., 2019
$\mu_{b}$	$(4.583 \times 10^{-4}, 6.922 \times 10^{-4})$	$5.94 \times 10^{-4}$	Manore et al., 2019
8	$\left(\frac{3.0}{1000*365}, \frac{4.5}{1000*365}\right) \text{day}^{-1}$	$\frac{3.7}{1000*365} \text{ day}^{-1}$	Desai et al., 2014
$\phi$	(0,1], varied	0.5	assumed
$1/\omega$	(28,370)	28 day	O'Meara et al., 2006; Teboh-Ewungkem et al., 2015
$\nu$	(0.01, 0.05)	0.01	O'Meara et al., 2006; Teboh-Ewungkem et al., 2015
1/a	(3,10)	5 days	O'Meara et al., 2006; Teboh-Ewungkem et al., 2015
$1/r_s$	constant	$1/6, 1/52  \mathrm{day}^{-1}$	O'Meara et al., 2006; Teboh-Ewungkem et al., 2015

 Table 5: Parameter values, ranges, and references that change across high/low transmission scenarios.

Parameter	Value Range	High Baseline	Low Baseline	Reference
$\kappa_v$	(0,1)	0.6	0.6	assumed
$\kappa_{b}$	(0,1)	0.6	0.6	assumed
$\sigma_a$	(1/365-1/20)	$1/33  day^{-1}$	$1/180 \; \mathrm{day^{-1}}$	Filipe et al., 2007; O'Meara et al., 2006
$\sigma_{\!\scriptscriptstyle S}$	(0.02 - 0.05)	$0.03~{\rm day^{-1}}$	$1/365^{-1}$	Filipe et al., 2007; O'Meara et al., 2006
$p_I$	1	1	1	Teboh-Ewungkem et al., 2015; Manore et al., 2019
$p_J$	[0, 0.5)	0.3	0.1	Teboh-Ewungkem et al., 2015; Manore et al., 2019
$\lambda_I, \lambda_J$	(0.15, 0.75)	0.5	0.7	O'Meara et al., 2006; Manore et al., 2019
$ \xi_{I_s} $	(0.1,1)	0.5	0.2	O'Meara et al., 2006; Teboh-Ewungkem et al., 2014; Baliraine et al., 2009; Manore et al., 2019
$\xi_{I_a}, \xi_{J_s}, \xi_{J_a}$	(0.1,1)	0.7	0.4	O'Meara et al., 2006; Teboh-Ewungkem et al., 2014; Baliraine et al., 2009; Manore et al., 2019
$\xi_{T_s}$	(0.1,1)	0.5	0.5	O'Meara et al., 2006; Teboh-Ewungkem et al., 2014; Baliraine et al., 2009; Manore et al., 2019
8	varied	$1.0137 \times 10^{-5}$	$2.8963 \times 10^{-6}$	Desai et al., 2014; Manore et al., 2019
$eta_{vh}$	(0.072, 0.64)	0.48	0.24	Chitnis et al., 2008
$eta_{hv}$	(0.010, 0.27)	0.022	0.022	Chitnis et al., 2008
m		3	1	Chitnis et al., 2008; Amek et al., 2012; Manore et al., 2019



### 2.2 Regional selection: Blantyre and Chikwawa, Malawi

We incorporate seasonality into the model discussed in Section 2, by linking regional average monthly temperature data in a year to temperature-dependent model parameters. The region-specific monthly temperature data is mapped to a time-linked parameter, yielding a realization of the parameter values at a given temperature during a specific time in the year. Two regions from Southern Malawi were selected for our investigative study to showcase our numerical results, one with low transmission and one with high transmission. The two regions, with malaria infections largely attributed to *P. falciparum*, are Blantyre district, a low transmission region, and the Chikwawa District, a high transmission region (Coalson et al., 2016). The country Malawi was chosen to showcase our specific results because it is a malaria endemic region with high malaria incidence and seasonal variation (Coalson et al., 2016), and also because of the diversity in transmission settings between neighboring districts. In 2017, there were over 5 million confirmed reported malaria cases in health facilities (about 4.9 million) and community level (just under a million), with even higher estimates at about 6 million and more (WHO, 2018). Interestingly, in (Coalson et al., 2016; Buchwald et al., 2017), it was reported that school aged children, aged 5–15 years, who make up about 30% of the population, had the highest prevalence compared to all other age groups, and hence seem to form the reservoir of infection (Buchwald et al., 2017). The study was based on data from the Malawian districts of Blantyre (a low transmission rural setting), Chikwawa (a low altitude, high transmission rural setting), and Thyolo (a high altitude, low transmission rural setting) (Coalson et al., 2016; Buchwald et al., 2017). Two of the mentioned regions are utilized in this study.

The first district, Blantyre, is a large urban area located in the highlands. It is reported to have relatively low malaria transmission (Coalson et al., 2016) with an entomological inoculation rate (EIR) for *P. falciparum* within the city of Blantyre around one infective bite/person per annum. However, a high proportion of city dwelling families make regular visits to nearby rural areas where some authors have reported estimated EIRs as high as 100 or more (Kariuki et al., 2013). The second region, the Chikwawa district, on the other hand is rural and known to have high malaria transmission. Because of the humidity and proximity of Chikwawa to the Shire river, the location makes it conducive for *Anopheles* mosquito breeding, which has been identified in the region (Coalson et al., 2016). The principal malaria mosquito vectors were identified as *An. arabensis*, *An. funestus*, and *An. gambiae s.s.* (Mathanga et al., 2012). An estimated EIR of 172 infectious bites per year have been reported in this region (Coalson et al., 2016; Mathanga et al., 2012). In a third study, Mzilahowa et al. (2012) collected 7,717 Anopheline mosquitos, of which 55.1% were *Anopheles gambiae* sensu lato and 44.9% were *Anopheles funestus*. In this study it was found that in Chikwawa the combined human blood index (an estimate of the proportion of mosquito blood meals obtained from humans) exceeded 92% and the *P. falciparum* sporozoite rate was 4.8% resulting in inoculation rates of 183 infective bites per person per annum, or a monthly rate of roughly 15 infective bites per person.

#### 2.3 Method to incorporate seasonality

In this section, we introduce our methodology that converts temperature-dependent parameters to time-varying parameters. In the context of malaria, temperature is known to impact key parameters related to mosquito demography and parasite development within the mosquito. In particular, mosquito biting rate, mosquito mortality rate, number of eggs laid per female mosquito per day, and the proportion of eggs that survive to adult mosquitoes (Mordecai et al., 2013; Miazgowicz et al., 2020) are mosquito demographic and physiological parameters impacted by temperature. Miazgowicz et al. (2020) performed an experiment on adult female A. Stephensi mosquitoes to compute daily per capita values for mortality, egg production, and biting rate at six constant temperatures: 16 to 36°C  $\pm$  0.5°C. Temperature significantly affected these trait values as illustrated in Figure 4. Likewise, these experiments demonstrated parasite development rates within the mosquito that increased with temperature (Figure 4).

Miazgowicz et al. (2020) presented empirically derived nonlinear thermal responses for several mosquito and parasite life-history traits. Their work updated and expanded on the work by Mordecai et al. (2013). The data from Mordecai et al. (2013) and from Miazgowicz et al. (2020) are shown in Figure 4. We modified the functional forms of Miazgowicz et al. (2020) to guarantee non-negative traits by redefining negative values to be zero. Using these functional relationships between temperature and mosquito demographic and parasite traits, we developed a data-driven method to link time of year to specific values for these non-constant parameters. In Section 4, we implement this method for two regions in southern Malawi with vastly different local transmission dynamics: Chikwawa (high-transmission) and Blantyre (low-transmission).

#### 2.3.1 Spline methodology

Here, we outline the steps to define a time-periodic parameter that is linked to a temperature-dependent parameter. Suppose we expect a temperature-dependent parameter to be roughly periodic with period  $\tau$ . To define a  $\tau$ -periodic function  $p_X(t)$  for the parameter related to a trait X, we proceed as follows:

1. Consider a *time* span of length  $\tau$  time units in which we have average *temperature* values,  $T_i$ , at times  $t_i$ , i = 0, ..., n, where n is the number of time points for which we have temperature data within the time interval  $\tau$ .

- 2. Define a function  $f_X : \mathbb{R}^+ \cup \{0\} \to \mathbb{R}^+ \cup \{0\}$  that maps temperature T to a non-negative real number for trait X.
- 3. Fit a cubic spline using the *spline* function in MATLAB 2020a, denoted  $s_X(t)$ , to the points  $(f_X(t_0), \dots, f_X(t_n), f_X(t_0))$ . We used evenly spaced knots representing months, where the time points  $t_i$  are converted into months via the expression  $t = \mod(t_i/30, 12)$ . The first point is duplicated to achieve continuity of the function defined over multiple years.
- 4. The time-periodic parameter related to trait X with period  $\tau$  is then defined as  $p_X(t) = s_X(\text{mod}(t,\tau))$  for all times  $t \in \mathbb{R}$ .

Note that in step 3 above, the first timepoint is duplicated at the end of the sequence so that  $p_X(t)$  is continuous.

#### 2.3.2 Implementation and application to two regions

In our model, we consider the traits X to be mosquito growth rate  $(m_g(t))$ , which is a function of the number of eggs laid per female per day and the proportion of eggs that survive to mature into adults; adult mosquito mortality rate  $(\mu_v(t))$ ; mosquito biting rate  $(\alpha(t))$ ; and parasite development rate (defined by pdr(t)). To apply the spline methodology to the temperature data for Chikwawa and Blantyre, we used average monthly temperature data from 1991–2016 for these regions (World Bank Group, 2019), defining  $t_i = i$  for i = 1, ..., 12. The temperature values and their distribution are represented by the grey bars as shown in Figures 5 and 6. Next, we map the temperature-dependent data for the traits and parameters (mosquito biting rate, mortality rate, eggs laid per female per day, percentage of eggs maturing into adults and parasite development rate) as given in (Mordecai et al., 2013; Miazgowicz et al., 2020) and illustrated in Figure 4, to the regional temperature data. For each trait, this yields temperature-dependent trait values at times  $t_i = i$  for i = 1, ..., 12, defined by the points of the coordinates of  $(f_X(t_1), ..., f_X(t_{12}))$ , for  $t_i = i$ , i = 1, ..., 12. Thus, for each of our study regions, we have values for each trait for each

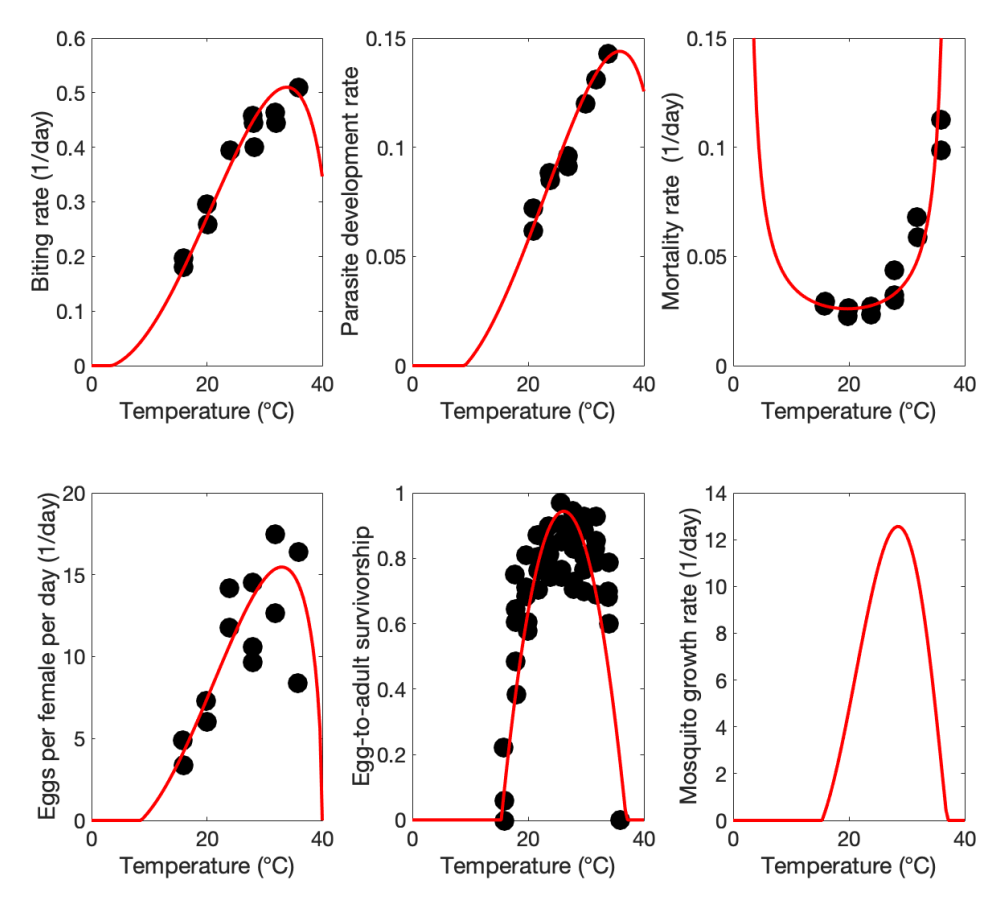


**Figure 4:** Temperature dependent mosquito and parasite life-history traits. The black dots are empirical data collected by Miazgowicz et al. (2020) and Mordecai et al. (2013) from various experiments and red curves are functional fits. Here we modified the functional fits from Miazgowicz et al. (2020) to guarantee that the traits remain non-negative. For the Mortality rate, we took the inverse of their data on mosquito lifespan. In order to estimate a function for mosquito growth rate (bottom right panel) we multiplied the functions fit in the previous two panels, the production rate of eggs per female per day and the egg-to-adult survivorship. Since this is not directly measured by experiment, there are no data points represented in the last panel.

month, each of which is directly linked to the temperature for that month. Next, we fit cubic splines (see Stoer and Bulirsch, 1980, Ch. 2),  $s_X(t)$ , to the points  $(f_X(1), \ldots, f_X(12))$  as discussed in Section 2.3.1 using the MATLAB 2020a *spline* function, extended from year to year. This yields a continuous time-periodic function  $(p_X(t))$  for each trait and parameter with period equal to one year. In essence, this data-driven function maps temperature-dependent mosquito and parasite development traits to time-dependent parameters, permitting the inclusion of fluctuating regional temperatures.

Plots of the values of the *temperature-dependent traits* for different *times* (*months*) are shown on the same graphs as the base historical temperature plots for Chikwawa and Blantyre in Figures 5 and 6. In these figures, the monthly average temperature values are given on the left *y*-axis, while corresponding monthly values of the traits and parameters are given on the right *y*-axis and illustrated by the bullet points, connected for ease of viewing only. For the base temperatures represented by the grey bars, the associated trait values are illustrated by the red bullet circles, •. For example, from Figure 5, in May (t = 5) where the average monthly temperature in Chikwawa is about 25°C, the biting rate is about 0.25 per day and the parasite development rate is about 0.075.

As part of our study, we are interested in how shifts in temperatures affect the entire malaria dynamics in our study regions. Thus, we also considered temperature shifts  $\Delta T$  of  $\pm$  1°C and  $\pm$  2°C. In these scenarios, we added  $\Delta T$  uniformly to the monthly temperatures  $T_i$  (but the new updated average temperatures are not shown). The new values of  $f_X(t_i)$  associated with either a  $\pm$  1°C or  $\pm$  2°C shift are computed as well as the new  $p_X(t)$  values. The trait values associated to the four temperature shifts are also illustrated in Figures 5 and 6, which shows their variations from the base date. The +1°C and +2°C related monthly trait values are illustrated by  $\times$  and  $\blacksquare$  bullets, respectively, while those for the -1°C and -2°C monthly trait values are respectively illustrated by + and  $\blacktriangle$  bullets.

Next, the *time-varying* periodic temperature-linked traits are incorporated into our model described by systems (1a)–(1g), (2), (3a)–(3c) and (4), yielding a **non-autonomous** system of ODEs. In the system, the parameters affected by temperature are mosquito mortality rate  $\mu_v(t)$ , transmission rates  $\beta_v(t)$  (from humans to vectors), and  $\beta_b(t)$  (from vectors to humans), and  $\Lambda_v(t)$ , the recruitment rate into the mosquito population. While the time-varying periodic trait for mosquito mortality directly gives us the time-varying periodic parameter values for mosquito mortality,  $\mu_v(t)$ , we need to obtain time-varying expressions for  $\beta_v(t)$ ,  $\beta_b(t)$ , and  $\Lambda_v(t)$ , using the time-varying traits obtained earlier. In particular, starting with the transmission rates, we define  $\beta_v(t)$  and  $\beta_b(t)$  as

$$\beta_v(t) = \beta_{vh} \alpha(t)$$
 and  $\beta_h(t) = \beta_{hv} \alpha(t) \left( \frac{pdr(t)}{pdr(t) + \mu_v(t)} \right)$ 

where  $\alpha(t)$  is the per-mosquito biting rate (with units of bites per mosquito per time) and  $\beta_{nh}$  is the number of mosquitoes that get infected given a bite on an infected host (with units of mosquitoes per bite), and so  $\beta_v$  has units of per time. This expression is a temperature-linked time-varying parameter, since  $\alpha(t)$  is a temperature-linked time-varying parameter as indicated in Figures 5 and 6. On the other hand,  $\beta_{bv}$  is the number of susceptible humans that get infected given a bite from an infected vector, with units of humans per bite. Hence, the function pdr(t) is the parasite development rate and  $\mu_v(t)$  is the mosquito death rate, each with units per time (in days) and both are temperature-linked time-varying parameters. Thus,  $\beta_b(t)$  is a more complex temperature-linked time-varying parameter with units of humans per mosquito per time. The expression  $\frac{pdr(t)}{pdr(t)+\mu_v(t)}$ links the extrinsic incubation period of the malaria parasite to transmissibility of the parasite from mosquitoes to humans. The mosquito has to be alive and the parasite in the mosquito must be at its transmissible form (sporozoite), for the parasite to be able to infect a susceptible human after a successful blood meal following a bite from an infected mosquito. Our methodology captures the increase in transmission potential based on the time period in the year, which is dependent on the temperature. For example, in the month of July (t = 7 months, corresponding to a time frame of  $t = t_7$  equal to 183–213 days), the base average temperatures in Chikwawa are at the lowest, about 22.5°C compared to the base average temperatures during the month of April (t = 4 months, corresponding to a time frame of  $t = t_4$  equal to 91–120 days), where the temperatures are higher than 25°C. From Figure 5, we see that in July (t = 7 months),  $\mu_v(t_7)$  is larger than the value in April,  $\mu_v(t_4)$ , while  $pdr(t_7)$  and  $\alpha(t_7)$  are both smaller than their respective April corresponding values,  $pdr(t_4)$  and  $\alpha(t_4)$ . Thus

$$\frac{\mu_v(t_7)}{pdr(t_7))} > \frac{\mu_v(t_4)}{pdr(t_4))}$$

so that

$$\alpha(t_7) \frac{pdrt_7)}{pdr(t_7) + \mu_v(t_7)} = \alpha(t_7) \frac{1}{1 + \frac{\mu_v(t_7)}{pdr(t_7))}} < \alpha(t_4) \frac{1}{1 + \frac{\mu_v(t_4)}{pdr(t_4)}} = \alpha(t_4) \frac{pdrt_4)}{pdr(t_4) + \mu_v(t_4)}$$

where  $t_4$  is the time frame in days corresponding to the month of April (4th month) and  $t_7$  is the time in days corresponding to the month of July (7th month). Thus,  $\beta_b$  is smaller in the month of July ( $\beta_b(t_7)$ ) than in the month of April ( $\beta_b(t_4)$ ), capturing the lower transmission potential within the human population in the colder months of July compared to the warmer month of April (National Malaria Control Programme, 2010).

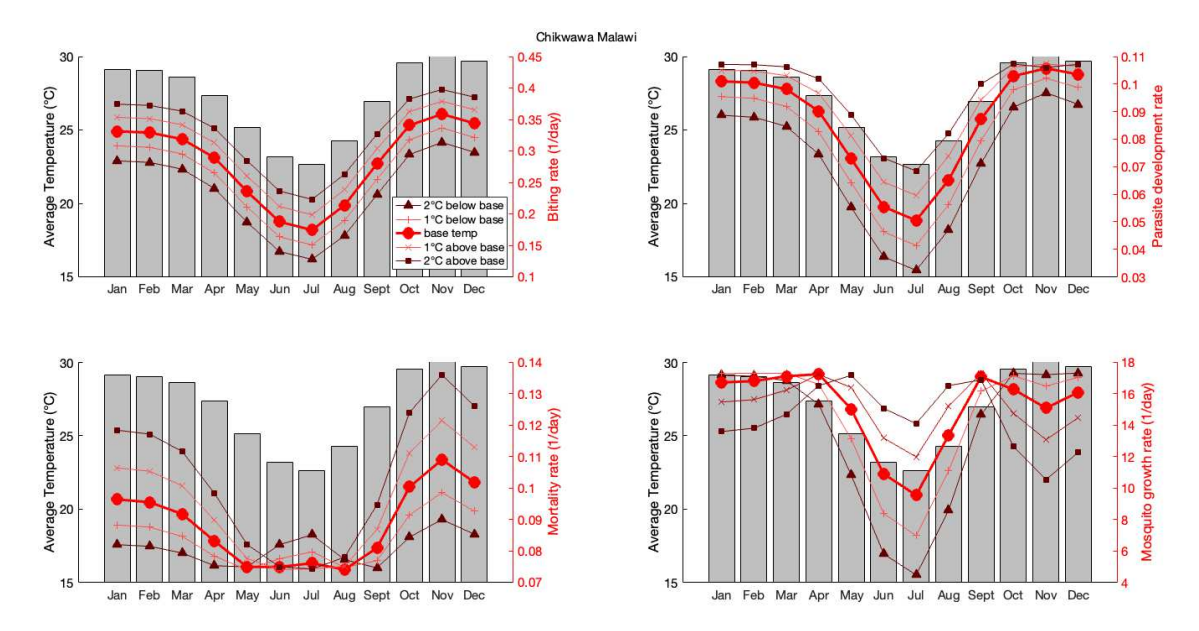


Figure 5: Seasonal mosquito and parasite traits for Chikwawa, Malawi. The grey bars plotted against a white background, show the average monthly temperature data from World Bank Group (2019) while the bullet points indicate trait values as determined by the correlations with temperature per the thermal relationships as shown in Figure 4, for mosquito biting rate, parasite development rate, mosquito mortality rate and mosquito growth rate. The red filled bullet, ●, shows the values corresponding to the base average monthly temperature data from World Bank Group (2019), while the × and ■ bullets indicate the monthly trait values when the average monthly temperature data from World Bank Group (2019) is increased by +1°C and +2°C respectively, meanwhile the + and ▲ bullets correspond to the cases when the monthly temperature data from World Bank Group (2019) is decreased by −1°C and −2°C. Note the nonlinear effects for the mortality rate and mosquito growth rate.

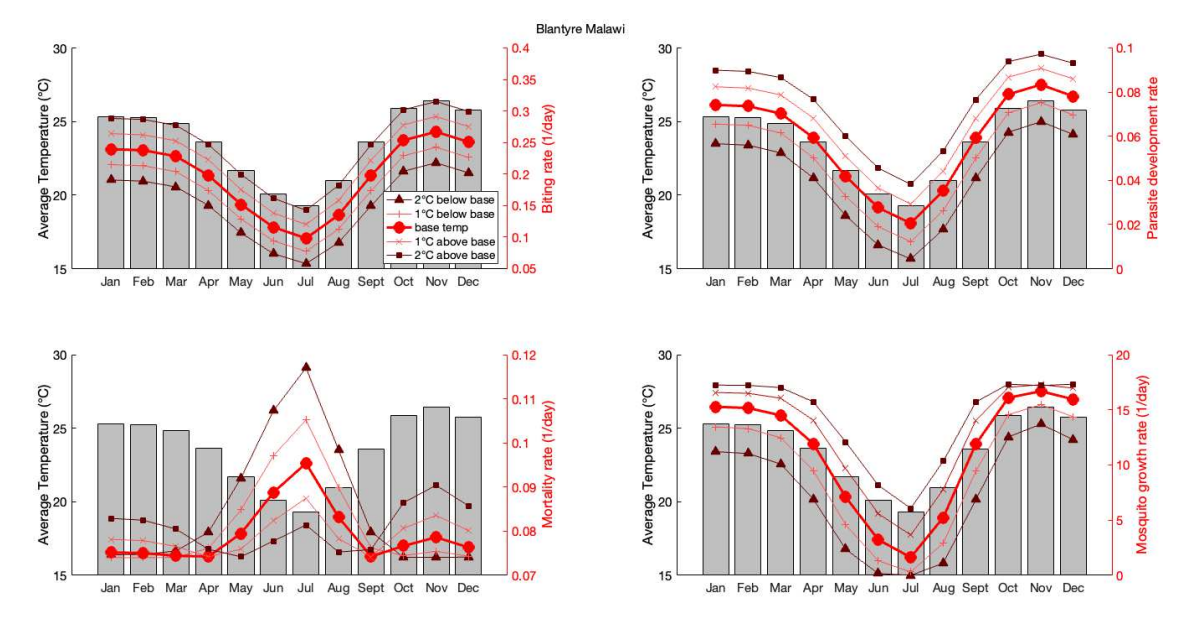


Figure 6: Seasonal mosquito and parasite traits for Blantyre, Malawi. The grey bars plotted against a white background, show the average monthly temperature data from World Bank Group (2019) while the bullet points indicate trait values as determined by the correlations with temperature per the thermal relationships as shown in Figure 4, for mosquito biting rate, parasite development rate, mosquito mortality rate and mosquito growth rate. The red filled bullet, ●, shows the values corresponding to the base average monthly temperature data from World Bank Group (2019), while the × and ■ bullets indicate the monthly trait values when the average monthly temperature data from (World Bank Group, 2019) is increased by +1°C and +2°C respectively, meanwhile the + and ▲ bullets correspond to the cases when the monthly temperature data from World Bank Group (2019) is decreased by −1°C and −2°C. Note the nonlinear effects for the mortality rate and that these effects are amplified for Blantyre as compared with Chikwawa.

Next, we discuss the recruitment rate into the mosquito population,  $\Lambda_v$ . This parameter, which is linked to the mosquito growth trait, depends on the number of eggs laid by a female mosquito and the proportion that survive the aquatic developmental stages, maturing to adult mosquito. We define  $\Lambda_v$  as

$$\Lambda_v(t) = b_v(t) \chi$$

where  $b_v(t) = p \, m_g(t)/2$  is the mosquito birth rate, and is a function of the number of eggs laid per female mosquito per day times the fraction of eggs that survive to mature into female mosquitoes modeled by  $m_g(t)$ . We assume 50% of the surviving mosquitoes are female. In our data and work, the egg to adult survival component of  $m_g(t)$  is considered to be the fraction of eggs that develop into adult mosquitoes under ideal conditions in the lab. In the wild, we would expect other extraneous factors to affect this survival proportion. Hence, we multiply  $m_g(t)$  by a field predation rate of eggs and larva, p. A value of p=0.04 was reported in (Kweka et al., 2011; Roux and Robert, 2019). To obtain the total mosquito recruitment rate from the per capita recruitment rate  $\Lambda_v(t)$ , we scale the mosquito recruitment rate by a parameter  $\chi$  such that when evaluated at the regional mean temperature  $\overline{T}$ , the number of female mosquitoes at the disease-free equilibrium will be equal to the desired mosquito-to-human ratio multiplied by the initial human population size; that is,  $\overline{\Lambda}_v \chi/\overline{\mu}_v = mN_b(0)$ , where  $\overline{\Lambda}_v$  represents the per capita mosquito recruitment rate and  $\overline{\mu}_v$  represents the mosquito death rate, both evaluated at the average yearly temperature. This yields  $\chi = mN_b(0)\overline{\mu}_v/\overline{\Lambda}_v$ . Under varying monthly temperatures, this results in a mosquito-per-human population that fluctuates around the initial ratio of mosquitoes to humans, m.

We computed the monthly entomological inoculation rate (mEIR) by integrating the number of infectious mosquito bites per human per unit time,  $\frac{\beta_v(t)}{N_b(t)} M_X \frac{pdr(t)}{pdr(t) + \mu_v(t)}$ , over each month, where here  $X \in \{s, r\}$  represents infection with either the sensitive or resistant malaria strain.

Embedding the aforementioned parameters into model system (1a)–(1g), (2), (3a)–(3c) and (4) yields a **non-autonomous** system of ODEs.

### 3 Threshold Number for Seasonal Malaria Transmission

In this section, we discuss threshold parameters associated with non-autonomous disease models. In autonomous disease models, the basic reproduction number  $\mathcal{R}_0$ , defined as the expected number of secondary infections caused by a primary infectious case in a fully susceptible population, is a threshold parameter that typically defines the threshold between a system trending towards a disease free equilibrium or not. In particular, a disease can become endemic (or an epidemic can occur) if and only if  $\mathcal{R}_0$  is greater than one (van den Driessche and Watmough, 2002) when the model does not exhibit a backwards bifurcation. For periodic models, which are non-autonomous, we need to tread with care. The basic reproduction number of the time-averaged autonomous system of a periodic model over a length of time may overestimate or underestimate infection risks (Bacaër and Guernaoui, 2006; Wang and Zhao, 2008). Hence, it is not a threshold number for the disease. For this reason we focus on the periodic threshold number rather than the time-averaged reproduction number.

The periodic threshold number over a period  $\tau$ , denoted  $\mathcal{R}_{0\tau}$  (Thieme, 2009), is only a biological reproduction number when the seasonality is removed. However,  $\mathcal{R}_{0\tau}$  does act as a threshold number describing the behavior of the system similarly to the reproduction number,  $\mathcal{R}_0$ , for an autonomous system.

Bacaër and Guernaoui (2006) introduced the concept of a basic reproduction ratio for periodic compartmental epidemic models by adapting the method of van den Driessche and Watmough (2002) to periodic systems that progress linearly along a chain of infected stages. The analysis of this ratio was extended by Thieme (2009) and Wang and Zhao (2008) with detailed analysis for more general non-autonomous systems of differential equations. Mitchell and Kribs (2017) provided explanations of the linear operator theory along with the necessary calculations. Mitchell and Kribs also showed under which conditions the time-averaged reproduction numbers would agree with the non-autonomous threshold number found by these linear operator methods. In Appendix A (see Supplemental Materials), we first derive this threshold number introduced by Mitchell and Kribs for our two-strain, non-autonomous malaria model. In Appendix B we provide formulation for the numerical computation of this threshold using the computational method of Posny and Wang (2014).

We have considered the case where the sensitive and resistant strains both exist in our high and low transmission regions. However, it may be that either the sensitive strain or resistant strain exist endemically alone in a region. The question remains: is it possible for the drug-resistant strain to invade a region populated endemically by a drug-sensitive strain? In Appendix C (see Supplemental Materials), we present the linear operator method outlined by Mitchell and Kribs (2019) for setting up the calculation for the invasion threshold number for periodic endemic models, and applied it to our seasonal malaria model. Note the nonlinear effects for the mortality rate and that it is amplified for Blantyre over Chikwawa. Appendix D contains the details for the computation of the necessary monodromy matrix and particulars for the application of the bisection method.



## 4 Model Simulations

In the simulations of the malaria model with seasonal temperature, we computed different model outputs using the baseline monthly temperatures in Chikwawa and Blantyre, and with those monthly temperatures varied from  $-2^{\circ}$ C up to  $+2^{\circ}$ C, in increments of  $1^{\circ}$ C. We investigated how these temperature shifts impact the seasonal reproduction number, the seasonal invasion reproduction number, monthly Entomological Inoculation Rate (mEIR), and the mean, likewise, amplitude of the oscillations observed.

We performed tests of the periodic threshold number  $\mathcal{R}_{0\tau}$ , with  $\mathcal{R}_{0\tau}$  computed following the method of Posny and Wang (2014) and as outlined in Appendix C (see Supplemental Materials), by integrating over the interval  $(0,\tau)$ , the equation for the evolution operator L as defined in Appendix C, Eq. (9). Approximately 100 time steps are used and the test is performed when both the sensitive and resistant strains are present, with periodic equivalence to  $\sqrt{\mathcal{R}_{\xi}\mathcal{R}_{\xi}}$ , where  $\mathcal{R}_{\xi}$  and  $\mathcal{R}_{\xi}$  are the reproduction numbers for the drug-sensitive and drug-resistant strain, respectively, for the autonomous problem. We combined the temperature data for the high transmission region, Chikwawa (Figure 5), and the low transmission region, Blantyre (Figure 6), associated with the mosquito data and calculated the periodic threshold numbers (see Figures 7 and 8 for the graphical illustrations). Both Figures 7 and 8 illustrate the results for a range of natural clearance ( $\phi$ ) values and resistant strain treatment efficacy factor ( $p_I$ ) values. The distinguishing factor between the two figures is that Chikwawa is a high transmission region while Blantyre is a low transmission region.

For both Figures 7 and 8, graph (a) shows the changes in  $\mathcal{R}_{0\tau}$  with changes in the natural clearance  $\phi$  and resistant strain treatment efficacy factor  $p_J$ , plotted for the baseline average temperature values from World Bank Group (2019). It is clear that  $\mathcal{R}_{0\tau}$  is largest for small values of  $\phi$  and  $p_J$ , as would be expected, since small  $p_J$ , respectively small  $\phi$  correspond to higher numbers of lingering resistant infections. However, note that the values for Blantyre (Figure 7 (a)) are typically lower when compared to the values for Chikwawa (Figure 7 (a)). The heat maps represented in graphs (b) and (c) of Figures 7 and 8 show the amount by which  $\mathcal{R}_{0\tau}$  is reduced when the baseline mean temperatures used in graphs (a) are reduced by 2°C, respectively, 1°C. Likewise, the heat map represented in graphs (d) and (e) show the amount by which  $\mathcal{R}_{0\tau}$  is increased when the baseline mean temperatures used in graphs (a) is increased by 2°C, respectively, 1°C. For both Blantyre and Chikwawa, the periodic reproduction threshold number increases as the mean monthly temperature increases. Overall,  $\mathcal{R}_{0\tau}$  values tend to be higher in the high transmission region of Chikwawa, when compared to the low transmission region of Blantyre.

Figure 9 illustrates how the seasonal invasion reproduction number,  $R_r^s$ , plotted using the baseline epidemiological parameters, changes with changes in temperature for both our low and high transmission settings.  $R_r^s$  is plotted, for temperature shifts in the range [-2, +2.5] °C, with the goal to highlight how temperature impacts the ability for the resistant strain to invade the sensitive strain's boundary equilibrium. The equilibrium sensitive population sizes as well as the parameters choices in the low and high transmission settings are different with or without temperature effects. Thus, the starting values for  $R_r^s$ , will differ in these two transmission settings and would depend on the parameter choices utilized for the two regions. The choice utilized shows that  $R_r^s$  < 1 in both regions, although the value for Chikwawa is for the most part higher.

Nonetheless, the values of  $R_r^s$  are increasing with increasing temperature shifts for both the low and high transmission regions, but still remain below one for all  $\Delta T$ . This indicates that the resistant strain is unable to invade the sensitive strain's boundary equilibrium in both low and high settings. While the rate of increase for the high transmission region, Chikwawa, is very gradual, the rate in Blantyre is steeper initially, increases from about 0.3 to 0.76. Eventually, the invasion number for Blantyre exceeds that of Chikwawa for temperature shifts of about +2 °C and higher. At  $\Delta T = +2$ °C, the invasion number becomes very similar to that of Chikwawa, despite the fact that its epidemiological parameters correspond to a lower transmission setting.

Our results indicate that the potential for the resistant strain to invade, while not possible, increases sharply and faster with increasing temperature in the low transmission region than in the high transmission region. This, we believe supports the proposal that resistant infections can easily be introduced in low compared to high transmission region, as depicted by the rate of increase of  $R_r^s$ , for low transmission region compared to the high transmission region as temperature shifts increase.

A commonly used epidemiological metric for malaria is the entomological inoculation rate (EIR): the number of infectious mosquito bites received by a human over a given time period, usually annually (aEIR) or monthly (mEIR). Here, we computed the strain-specific mEIR for each transmission region over the course of three years (see Figure 10), and for temperature shifts  $\Delta T \in \{-2, -1, 0, +1, +2\}$  degrees Celsius. An estimated EIR of 172 infectious bites per year have been reported in Chikwawa (Coalson et al., 2016; Mathanga et al., 2012), the equivalent of roughly 14 infectious bites per month. Similarly, Mzilahowa et al. (2012) sampled mosquitoes over 52 weeks from January 2002 to January 2003, in two villages in Chikwawa district. They found that 55.1% were *Anopheles gambiae* sensu lato and 44.9% were *Anopheles funestus*. Additionally, the combined human blood index exceeded 92% and the *P. falciparum* sporozoite rate was 4.8%, resulting in aEIR estimates of 183 (infected bites/year), i.e. an mEIR of about 15 (infected bites/month). In the densely populated urban city of Blantyre, the aEIR has been estimated to be about one infective bite per person per year, equivalent to a monthly average of about 0.08, however a large proportion of individuals in this region regularly visit neighboring rural areas with aEIRs over 100 (Kariuki et al., 2013). This may explain why malaria persists throughout the year in this region. Our simulations produced comparable mEIRs ranging from roughly three

to eleven at baseline temperatures for Chikwawa, and between zero and 0.065 for Blantyre (Figure 10). The majority of those infectious bites result from mosquitoes infected with the sensitive strain.

Chikwawa is subject to oscillations that increase in amplitude from -2 to 0 degree shifts, as shown in Figure 10. However, as temperature is further increased, the peaks in the mEIR remain fairly similar, with the troughs becoming more shallow, resulting in higher total infectious bites per person over the course of three years. At  $\Delta T = +2^{\circ}$ , these oscillations appear irregular in comparison to cooler temperature regimes. The mEIR at  $\Delta T = +2^{\circ}$ , is highly suggestive that Chikwawa has moved from seasonal transmission to perennial transmission.

In Blantyre, although the seasonal reproduction number is less than one for each temperature shift, increasing temperatures allow malaria to persist longer, and with higher amplitude oscillations. For example, a two degree increase in temperature from baseline increased mEIR from nearly zero to approximately 0.2 by the end of year three in Blantyre.

Because the invasion reproduction number,  $R_r^s$ , is less than one for temperature shifts  $\Delta T \in [-2^{\circ}\text{C}, 2^{\circ}\text{C}]$ , we expect only the sensitive strain to persist as time tends to infinity. Figure 11 captures the periodic dynamics of the asymptotically stable limit cycles in Chikwawa when only the sensitive strain is present. As the temperature shift  $\Delta T$  increases from  $-2^{\circ}\text{C}$  to  $+2^{\circ}\text{C}$  from baseline, the cycles shift to increasing values, however, the amplitudes of those cycles change in a non-monotonic fashion. The largest amplitude oscillations are observed at intermediate temperature shifts of  $\Delta T \in \{-1^{\circ}\text{C}, 0^{\circ}\text{C}\}$ . In contrast to the simple closed curves occurring between -2 and +1 degree temperature shifts, at the highest temperature shift of  $\Delta T = +2^{\circ}\text{C}$ , we observe qualitatively different cycles, with multiple peaks within a one year period of different magnitudes. Similar to our observations of the mEIR, the peaks of the oscillations are similar at 0 and +1 degree shifts, but the trough is more shallow at the +1 degree temperature shift. Finally, the peak in infected mosquitoes is smaller at  $\Delta T = +2^{\circ}\text{C}$  than for  $\Delta T = +1^{\circ}\text{C}$ . In fact, the highest peak prevalence in mosquitoes occurs at 0 and +1 degree shifts. This is likely a consequence of the non-monotonic relationship between mosquito and within-mosquito parasite demographics with respect to temperature and the fact that the temperatures in Chikwawa exceed the optimal temperatures for malaria transmission during parts of the year.

Although only the sensitive strain persists in the long run using our baseline monthly temperatures and epidemiological parameter values, the sensitive and resistant strain can simultaneously persist for certain regions of the  $(p_J, \phi)$  parameter space (and

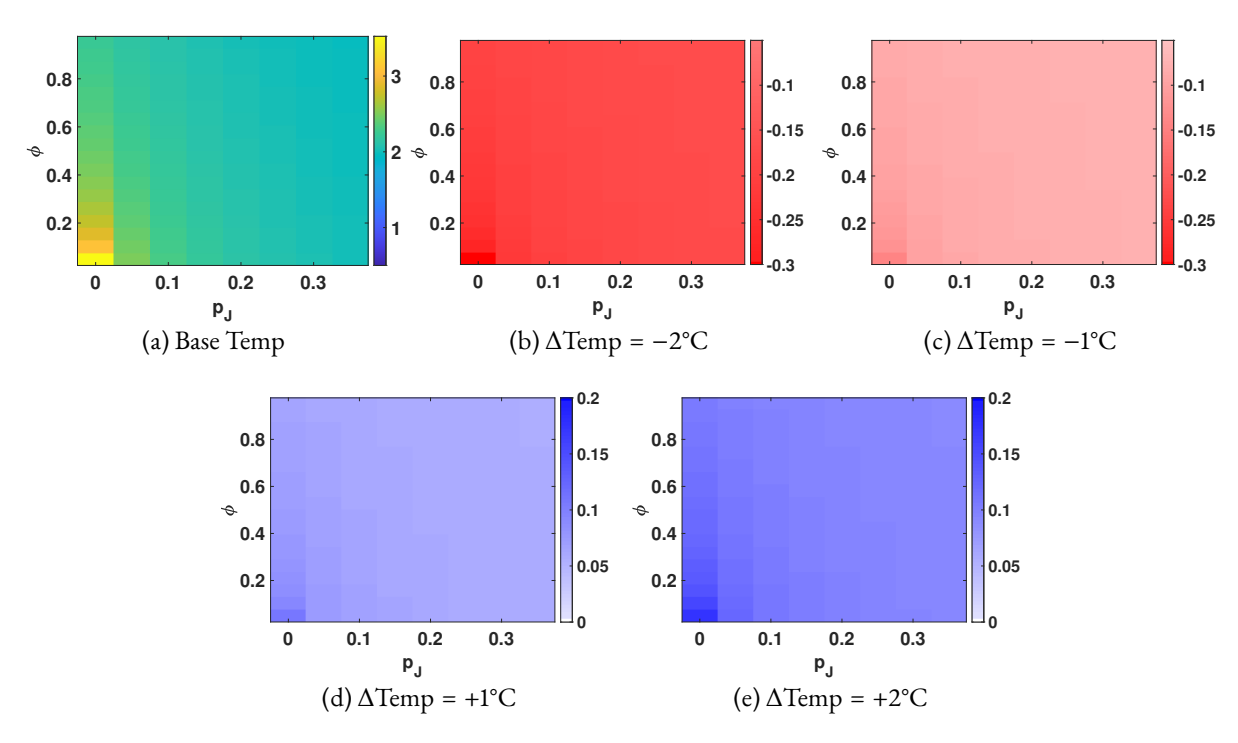


**Figure 7:** Heatmaps showing  $\mathcal{R}_{0\tau}$  for Chikwawa plotted for different values of  $\phi \in (0,1]$ , the scale factor that reduces the rate of natural clearance of resistant parasites relative to the sensitive parasite, and  $p_J$ , where  $0 \le p_J < .4$ , is the efficacy of treatment for a resistant strain infection. Subfigure (a) illustrates the value of  $\mathcal{R}_{0\tau}$  for the base average monthly temperatures per World Bank Group (2019). The subfigures (b) and (c) show the decrease in  $\mathcal{R}_{0\tau}$  resulting from a uniform two and one degree temperature decrease from the baseline, respectively. (d) and (e) demonstrate an increase in  $\mathcal{R}_{0\tau}$  resulting from a uniform one and two degree increase from the base temperatures, respectively. The red in figures (b) and (c) indicates a net decrease in  $\mathcal{R}_{0\tau}$  at the new temperature from the base.

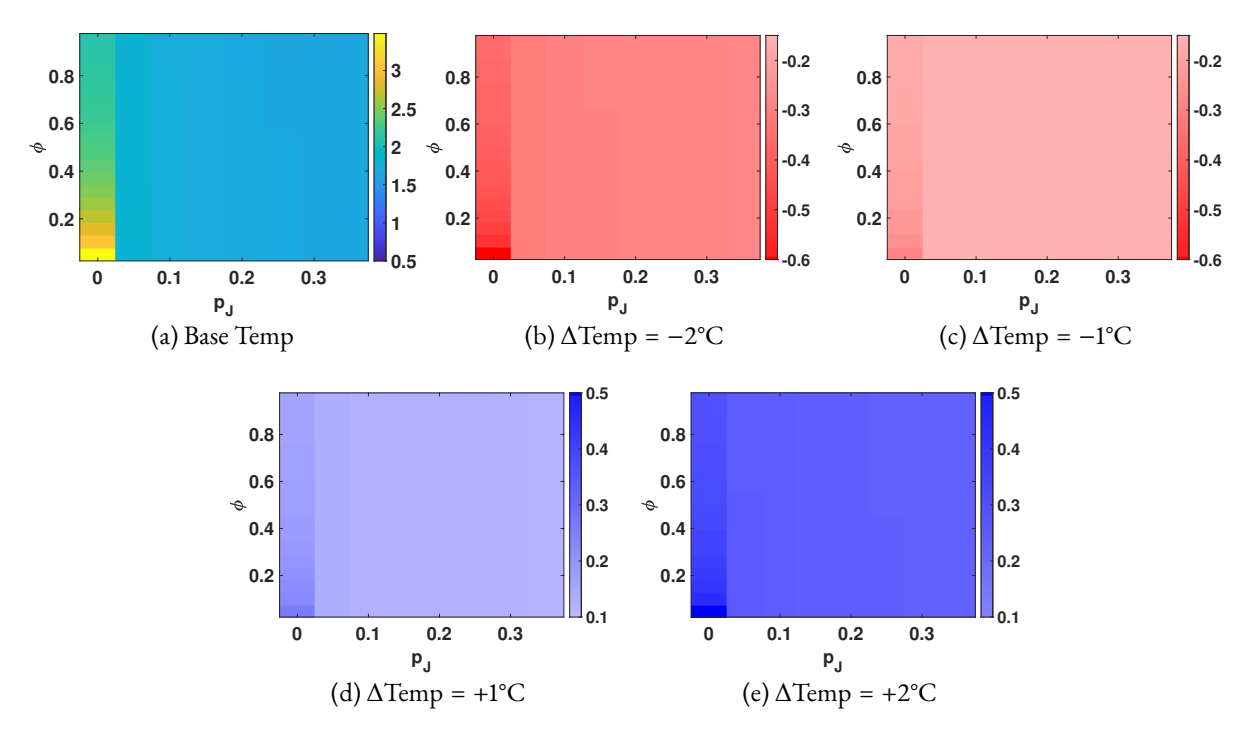


**Figure 8:** Heatmaps showing  $\mathcal{R}_{0\tau}$  for Blantyre plotted for different values of  $\phi \in (0,1]$ , the scale factor that reduces the rate of natural clearance of resistant parasites relative to the sensitive parasite, and  $p_J$ , where  $0 \le p_J < .4$ , is the efficacy of treatment for a resistant strain infection. Subfigure (a) illustrates the value of  $\mathcal{R}_{0\tau}$  for the base average monthly temperatures per World Bank Group (2019). (b) and (c) show the decrease in  $\mathcal{R}_{0\tau}$  resulting from a uniform two and one degree temperature decrease from the baseline, respectively. (d) and (e) demonstrate an increase in  $\mathcal{R}_{0\tau}$  resulting from a uniform one and two degree increase from the base temperatures, respectively. The red in figures (b) and (c) indicates a net decrease in  $\mathcal{R}_{0\tau}$  at the new temperature over the base. The blue in (d) and (e) indicates a net decrease in  $\mathcal{R}_{0\tau}$  at the new temperature from the base.

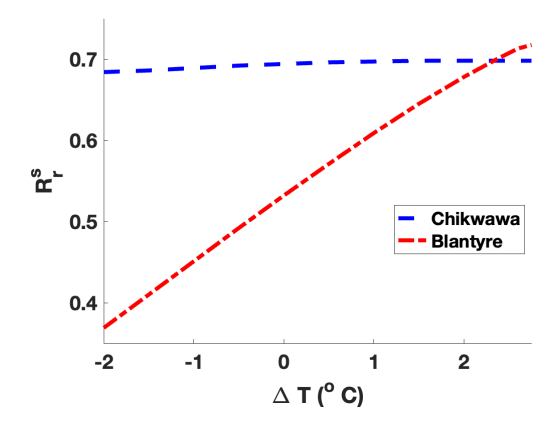


**Figure 9:** Plot of the invasion reproduction number of the resistant parasite strain at the sensitive parasite strain's equilibrium (boundary equilibrium), plotted for different temperature shifts in the range [-2, +2.5] ° C. The red dot-dashed curve shows the behaviour for Blantyre; the blue dashed curve shows the behaviour for Chikwawa. We see that  $R_r^s < 1$  for both regions but increases with increasing temperatures, with the rate for Blantyre, the low transmission region, faster than that for Chikwawa.

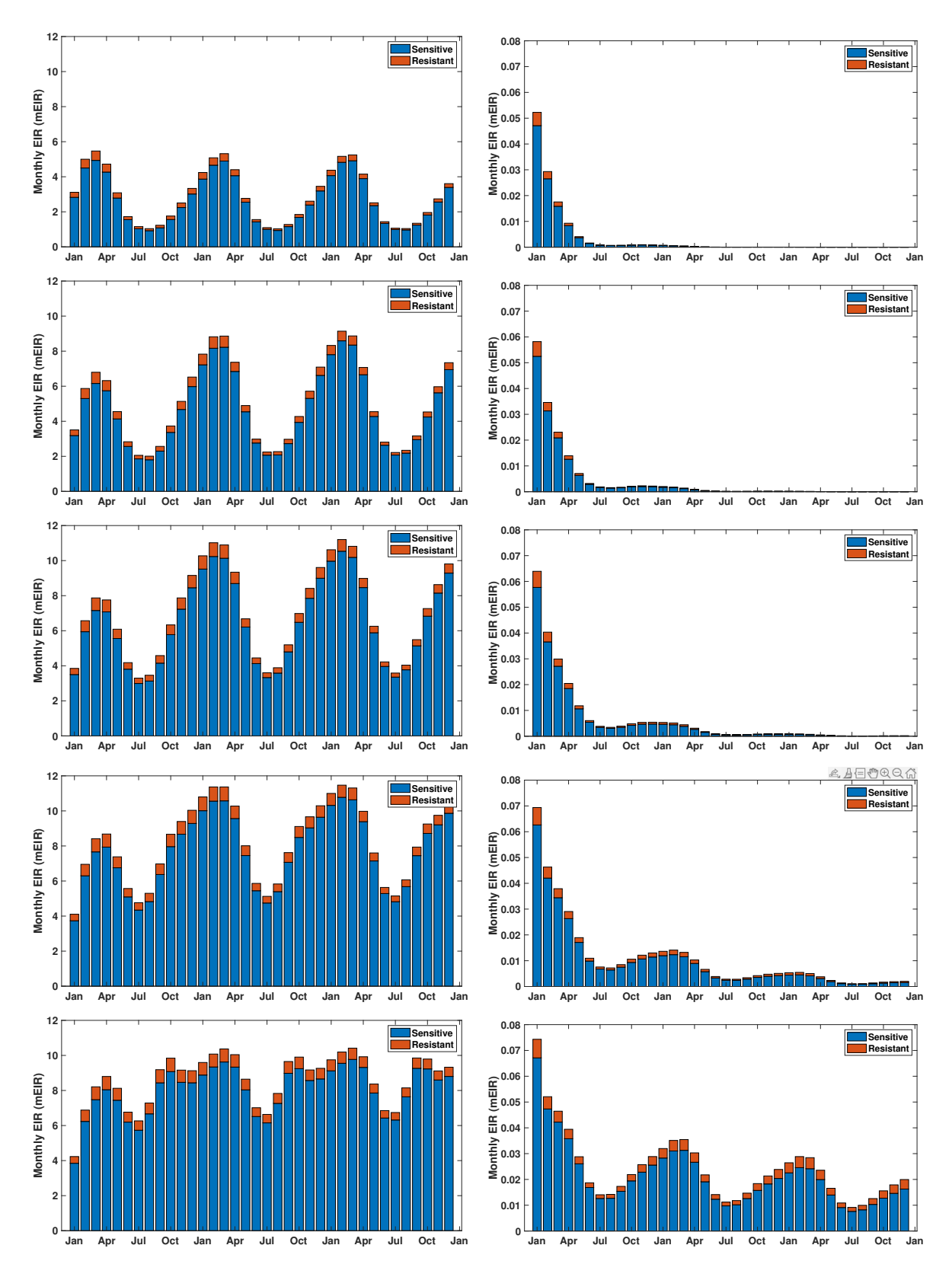


**Figure 10:** Monthly Entomological Inoculation Rate (mEIR) in years 1–3 of the simulation for Chikwawa (left column) and Blantyre (right column). Each row represents the mEIR for a different temperature regime (temperatures increase with each row). (Row 1) Two degrees cooler; (Row 2) One degree cooler; (Row 3) Baseline temperatures; (Row 4) One degree warmer; (Row 5) Two degrees warmer.

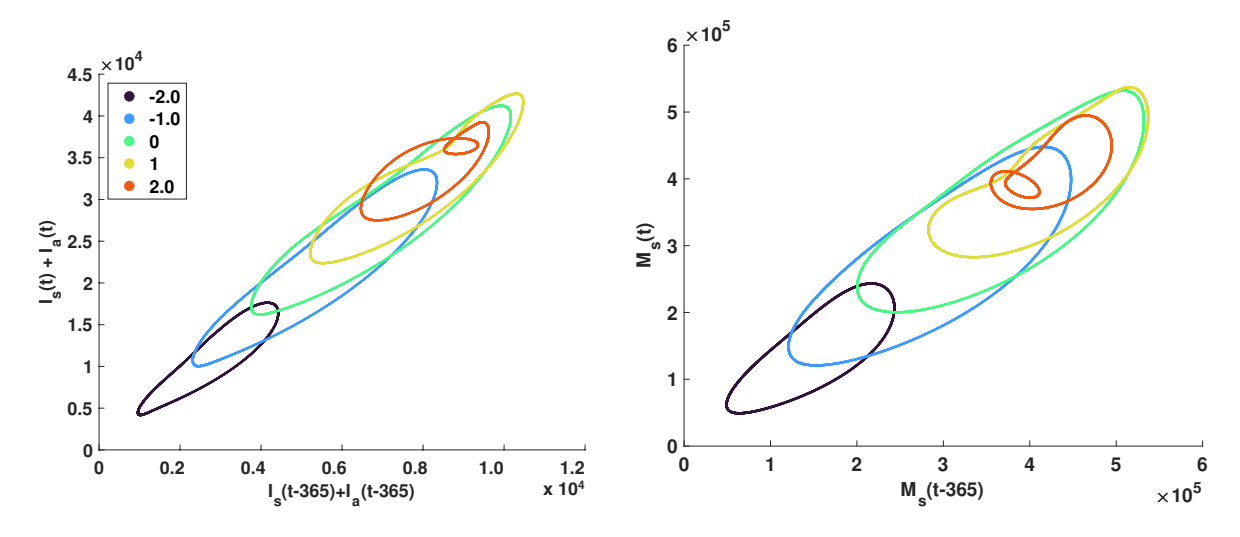


**Figure 11:** Sensitive Strain periodic cycles in Chikwawa for temperature shifts  $\Delta T \in \{-2, -1, 0, +1, +2\}$  degrees Celsius.

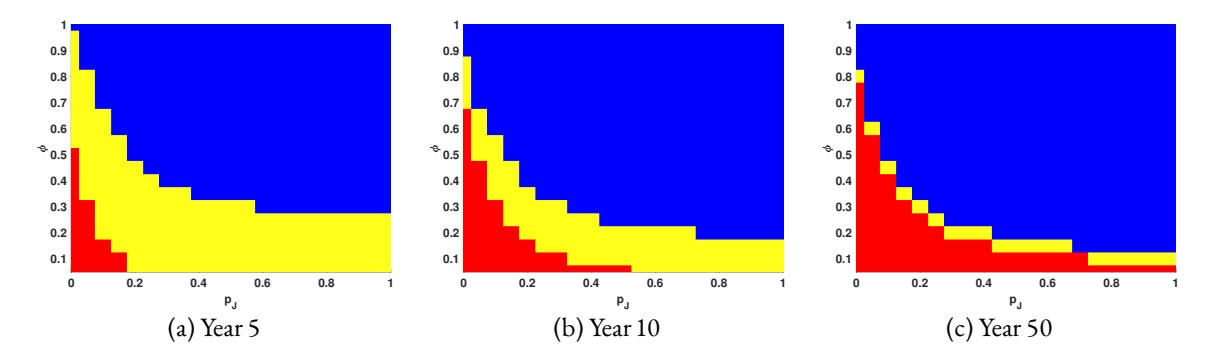


**Figure 12:** Regions of the  $(p_J, \phi)$ -parameter space, where  $p_J$  is the efficacy of treatment for a resistant strain infection and  $\phi$  is the scale factor that reduces the rate of natural clearance of resistant parasites relative to the sensitive parasite, are colored according to whether sensitive (blue), resistant (red), or both strains (yellow) persist in year 5 (a), year 10 (b) and year 50 (c) of the simulation for Chikwawa. The criterion for persistence is the presence of more than one infected individual of that type. Baseline monthly temperatures are used.

every other parameter set to their baseline values). Recall that  $p_J$  denotes the efficacy of drugs used to clear resistant infections, and  $\phi$  denotes a scale factor that reduces the rate of natural clearance of resistant parasites relative to sensitive parasites. Therefore, we expect to observe more resistant infections when  $p_J$  and  $\phi$  are small. Figure 12 indicates the regions of this parameter space for which one or both strains persist (defined as having a value above 0.2 per 100,000 individuals) after five, ten, and fifty years of the simulation. Sensitive-only is indicated in blue, resistant-only is indicated in red, and the presence of both strains is indicated in yellow. Over time, the coexistence region in the  $(p_J, \phi)$  parameter space narrows. We note that our baseline values of  $p_J$  and  $\phi$  lie close to this boundary. Large values of  $p_J$  and  $\phi$  are more likely to lead to the sensitive-strain dominating, while low values of these parameters tend to lead to the resistant strain dominating. After 50 years, the transition between these two regimes becomes abrupt, suggesting that the system is highly sensitive to the value of these parameters for intermediate values.

Our results at baseline monthly temperatures for Chikwawa and baseline epidemiological parameters suggest a non-monotonic relationship between transmission potential (measured by mEIR) and the temperature shift  $\Delta T$ . However, Figure 13, which shows the change in cases per 100,000 individuals for each infected state ( $I_s$ ,  $I_a$ ,  $J_s$ ,  $J_a$ ) at different temperature shifts  $\Delta T \in \{-2, -1, +1, +2\}$  degrees Celsius after 50 years, indicates that for prevalence, this non-monotonicity only occurs near the boundary between sensitive-strain dominance and resistant-strain dominance. Away from this boundary, cooler temperatures lead to decreased prevalence in both resistant and sensitive infections, while warmer temperatures lead to increased prevalence in both resistant and sensitive infections, both symptomatic and asymptomatic.

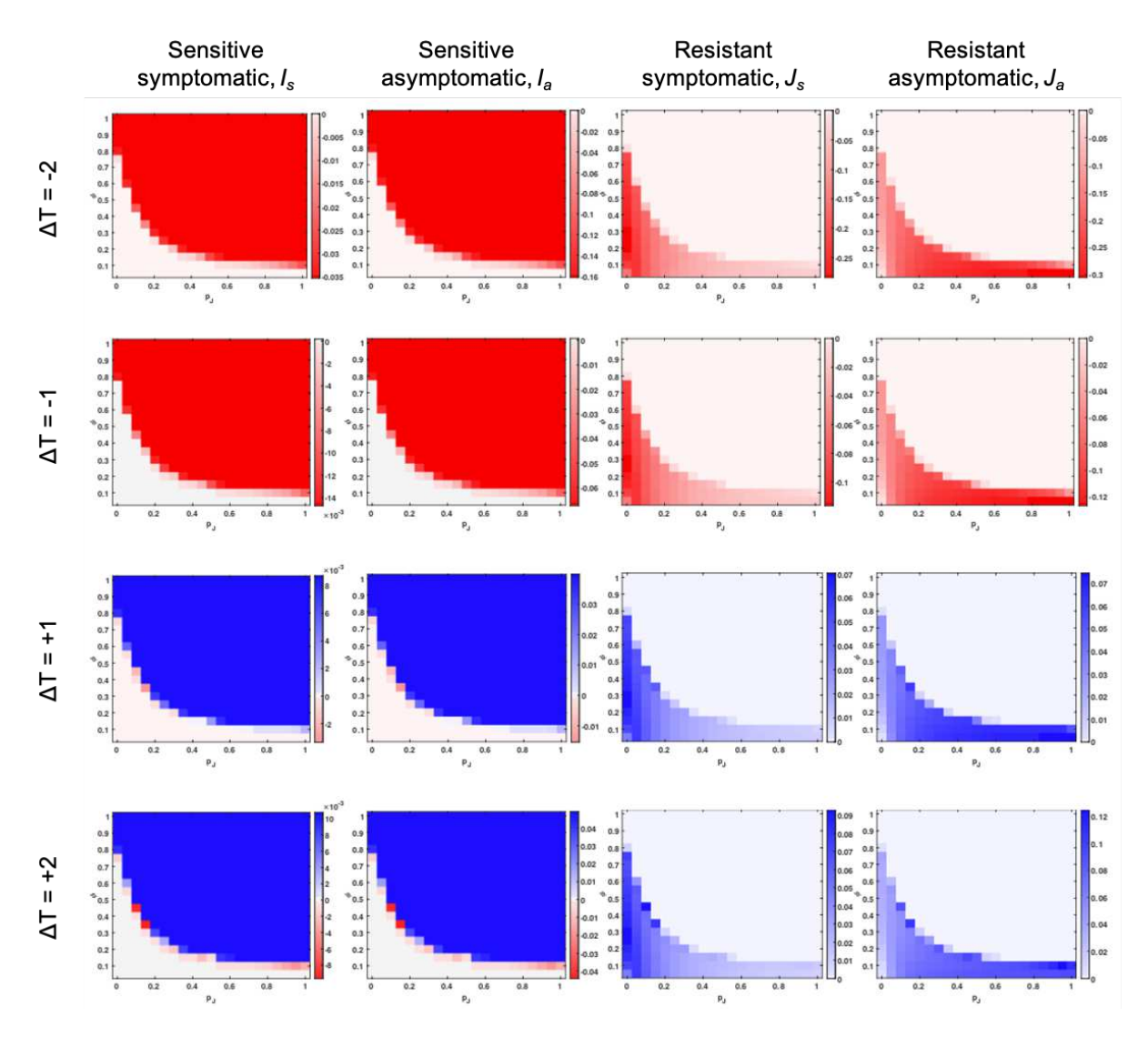


**Figure 13:** Change in  $I_s$  (first column),  $I_a$  (second column),  $J_s$  (third column),  $J_a$  (fourth column) infected individuals per 100,000 in Chikwawa with seasonal temperature. Row 1: two degree decrease; Row 2: one degree decrease; Row 3: one degree increase; Row 4: two degree increase. The color blue corresponds to an increase in disease prevalence, and the color red corresponds to a decrease. Each subfigure is shown as a function of  $(p_J, \phi)$ -parameter space, where  $p_J$  is the efficacy of treatment for a resistant strain infection and  $\phi$  is the scale factor that reduces the rate of natural clearance of resistant parasites relative to the sensitive parasite.



## 5 Conclusions

Climatic factors such as temperature, rainfall and humidity are key components to the regions and locality where malaria transmission occurs, with temperature a very critical component (CDC, 2020). In particular, low temperatures thwart Anopheles mosquito survival and population growth and impede a successful completion of the malaria parasite growth and infection cycle (CDC, 2020). Additionally, regions where malaria elimination has been successful risk re-introduction of the disease, with a higher risk for temperate regions such as Western Europe and parts of the US as these regions harbor the malaria transmitting Anopheles species mosquitoes (CDC, 2020). In fact, the aforementioned is true for many other mosquito-borne diseases, with observable seasonal trends and variable disease transmission burden associated to temperature and the locality, as well as the fact that shifting climatic patterns is affecting mosquito abundance and redistribution (Roth et al., 2019; Shapiro et al., 2017).

Following our preceding discussion and the recent World Malaria Report showing an increase in malaria cases and deaths over the past reporting period worldwide (WHO, 2021a), we set out to understand temperature effects on malaria transmission, proposing a methodology that utilizes reported monthly local temperature data capturing the regional effects. To do so, we proposed a two strain, drug-sensitive and drug-resistant, malaria transmission model that can be applied to different malaria transmission regions, using the actual reported temperature data for the region and its current characterization of its transmission state of high or low transmission region. We incorporated temperature effects into our malaria model by mapping mosquito and parasite temperature-linked traits and parameters to time-varying traits and parameters using regional average temperatures as the connector. The embedding of the time-varying parameters into our model yielded a system of non-autonomous ordinary equations. We then demonstrated our methodology and technique on two regions in Malawi, one a high transmission region (Chikwawa) and the other a low transmission region (Blantyre) and investigated the impact of seasonality on malaria transmission dynamics and burden in these regions. We computed monthly entomological inoculation rates and the number of malaria infections over a three year period for each of the regions.

Our results (see Figure 10) coincide with what is observed in Chikwawa, Malawi (Weather Climate Online, 2021) for the base reported temperatures, higher disease burden and malaria cases during the months of January to April where the temperatures are between 25°C and 28°C, compared to the months of May to June where the temperatures are lower, typically less than 25°C, with the peak season in January. While we did not explicitly include rainfall, we believe that its embedding into our model is implicit through our capture of the monthly distribution of the parameter traits and values associated to mosquito growth and survival, as well as with the within-mosquito parasite development. For example the months of January to April are also the rainy season months in Chikwawa with rainfall occurring on almost every day during these periods. Hence, if the rainfall is not as heavy so as to wash away mosquito breeding grounds, then these months provide ideal temperatures and rainfall for mosquito growth and development, hence contributing to the observed increase in disease burden, per the illustrated monthly Entomological Inoculation Rates (mEIR) as in Figure 10, during these months. On the other hand, the months of May to July are the drier months and the temperatures are lower, typically less than 25°C. Rainfall during each of these months occur on fewer than 4 days, with about 8 days in May (Weather Climate Online, 2021; World Bank Group, 2019). Thus, these conditions are not optimal for mosquito survival and growth, and cooler temperatures slow parasite development—in a laboratory study it was reported that mosquito lifespan was between 3 and 6 weeks, but typically shorter under natural conditions, and the time frame for parasite development was reported to be  $\approx 14$  days at 26°C and  $\approx 30$  days at 20°C (Baton and Ranford-Cartwright, 2005). For each of the months of August to November where the temperatures are on the rise, peaking in November at about 30°C, the number of days in which rainfall is reported is less than 4, with about 11 days in November (Weather Climate Online, 2021; World Bank Group, 2019). Thus, these conditions are again not generally as ideal with November being the time period with highest mosquito mortality. But this is compensated for with higher biting rate and parasite development rate. Thus, even though mosquito mortality is higher in November compared to the May-July period, mosquito growth rate is higher in November than in those months of May-July. In Blantyre, we also observe a peak season occurring during the month of January for the base temperature, but overall, given that temperatures are lower in Blantyre, the malaria burden is lower. We note that in the future we would incorporate rainfall effects since other regions may not exhibit the nice one-to-one correspondence between the rainy and dry seasons and temperature.

Given that mean monthly temperatures are changing as a result of shifts in temperatures due to global climate change, we used our model to investigate the impact of temperature shifts on disease burden in the the range [-2, +2] degrees Celsius for our two studied regions. What is evident is the increased activity with a  $+2^{\circ}$ C increase in base average monthly temperature resulting in higher monthly Entomological Inoculation Rates (mEIR) for Blantyre with peaks around the month of January compared to the base cases, and a much lower activity associated to a  $-2^{\circ}$ C decrease in base average monthly temperature (see Figure 10). Moreover, the proportion of resistant infections is higher for the  $+2^{\circ}$ C scenario which may have dire consequences for malaria control and mortality in this region, since most malaria disease-induced deaths are typically from the population of especially among naive-immune and non-immune individuals (Teboh-Ewungkem et al., 2015; Manore et al., 2019). Similar increases are seen for Chikwawa, but interestingly, we see that for a  $+2^{\circ}$ C increase in temperature, there is a shift in the peak season month to about March with the emergence of a second smaller peak around the month of December.

In all, our results capture the effects that fluctuating seasonal temperature and shifts in seasonal temperatures in the range [-2, 2] degrees Celsius, have on malaria transmission dynamics and burden in a high and low transmission regions in Malawi, captured through the computed mEIR. We note that our model which was not tuned to fit the measured mEIR, closely depicts the values reported in Blantyre and Chikwawa (Coalson et al., 2016; Makanga and Krudsood, 2009; Kariuki et al., 2013). Another way in which we captured the malaria transmission potential and burden was via our computed periodic time-dependent threshold (reproduction) showing that the resistant parasite strain would die out more quickly when we have partial resistance in that the malaria parasite is not totally refractory to the the antimalarial drug used for treatment (that is  $p_I$  is not close to zero and relatively high, more towards its high value used), and also when the scale factor  $\phi$  is high.

Since drug-resistant parasite strains are an ever present concern in malaria endemic regions, we also investigated possible coexistence between a sensitive malaria strain and a resistant malaria strain within the temperature ranges noted, assessing malaria
disease risks in relation to temperature shift. This was also the impetus for calculating the periodic threshold invasion number
using the baseline temperatures and corresponding parameters to assess the ability of the resistant parasite strain invading the
sensitive strain boundary equilibrium; our results showed that the resistant strain could not invade the sensitive strain boundary
equilibrium based on our model even with temperature shifts in the range [-2, +2] degrees Celsius. However, even though
impossible, the potential to invade increases with increasing temperature for both Chikwawa and Blantyre, even though that
increase is faster in Blantyre, the low transmission region, than in Chikwawa, the high transmission region. The fact that the
resistant strain cannot invade the sensitive strain's equilibrium is also captured in our model in that in the long run the sensitive
strain out-competes the resistant strain and remains the strain that persists (see Figure 12). However, transient dynamics shows
that in the short term, the two strains can coexist, with the sensitive strain being the dominant strain. How refractory the resistant
strain is to the anti-malarial drug is key, as fully resistant parasites ( $p_f \approx 0$ ) have a higher chance to persist in the short term, even
if the scale factor that reduces the rate of natural clearance of resistant parasites relative to sensitive parasite is relatively high. The
key takeaway is that continuous monitoring of malaria is essential.

Our results indicated that the resistant strain would not be able to invade the sensitive strain steady-state in Blantyre or Chikwawa under the baseline parameter assumptions, regardless of the temperature shifts considered in this work. There is, however, debate regarding what we should expect to occur in a low versus a high transmission setting. One viewpoint is that a resistant strain is better able to establish in a low transmission setting, but once established in a high transmission setting, will spread more quickly. Bushman et al. (2018) developed an individual-based model to explore factors that could explain this phenomenon, and identified natural immunity and coinfection as possible explanations. On the other hand, Talisuna et al. (2007) note that there is controversy regarding whether transmission intensity actually impacts the ability for drug resistance to evolve and spread. We surmise that the answer to this question, where does resistance take hold and/or spread more easily, is very region specific, and its interaction with seasonality is likely very complex given the nonlinear impact of temperature on mosquito and parasite dynamics, their interaction, and the subsequent implications for malaria transmission. To properly study this topic, it would be important to include dynamic immunity feedback and the possibility of co-infection.

An important aspect of our work is that the spline methodology used gives a means to apply our model for seasonal transmission without forcing a sinusoidal fit to the data. This approach incorporates the natural spatial variation seen in malaria endemic regions and we believe our methodology is novel. It is easily transferable to other models and can be used to capture seasonal effects on diseases in different regions.

Future work involves the incorporation of rainfall data to capture various regions including those for which the rainfall and temperature data are out of sync. We also plan to develop individualized forecasting tools for malaria control in various regions, incorporating intermittent preventative treatment (IPT) into the model by capturing the local transmission levels and seasonal temperature profile.

## **Acknowledgments**

OP was supported by the National Science Foundation (NSF) under Grant Nos. DMS-1953838 and DMS-2045843. MR was also supported under DMS-1953838. KG was supported by the NSF under Grant Nos. DMS-1814659 and DMS-2000044. MIT-E was supported by the NSF under Grant No. DMS-1815912. MIT-E also acknowledges support from Johnson and Johnson WiSTEM2D Scholars program. AP was supported by the NSF under Grant No. DMS-1815750. ZF was supported by the NSF under Grant No. DMS-1814545. Research presented in this article was supported by the Laboratory Directed Research and Development program of Los Alamos National Laboratory under project numbers 20190581ECR and 20210062DR and supported CM and MR. The authors acknowledge the support of an American Institute of Mathematics SQuAREs grant.



## References

- Adegboye, M. A., J. Olumoh, T. Saffary, F. Elfaki, and O. A. Adegboye (2019). Effects of time-lagged meteorological variables on attributable risk of leishmaniasis in central region of Afghanistan. *Science of The Total Environment 685*, 533–541. 5
- Agusto, F. B. (2020). Optimal control and temperature variations of malaria transmission dynamics. *Complexity 2020*, 5056432. 4
- Agusto, F. B., A. B. Gumel, and P. E. Parham (2015). Qualitative assessment of the role of temperature variations on malaria transmission dynamics. *Journal of Biological Systems 23*(04), 1550030. 4
- Amek, N., N. Bayoh, M. Hamel, K. A. Lindblade, J. E. Gimnig, F. Odhiambo, K. F. Laserson, L. Slutsker, T. Smith, and P. Vounatsou (2012). Spatial and temporal dynamics of malaria transmission in rural western Kenya. *Parasites & Vectors* 5(1), 86. 10
- Artzy-Randrup, Y., D. Alonso, and M. Pascual (2010). Transmission intensity and drug resistance in malaria population dynamics: implications for climate change. *PloS one 5*(10), e13588. 5
- Bacaër, N. and S. Guernaoui (2006). The epidemic threshold of vector-borne diseases with seasonality, the case of cutaneous leishmaniasis in Chichaoua, Morocco. *J Math Biol 3*, 421–436. 15
- Baliraine, F. N., Y. A. Afrane, D. A. Amenya, M. Bonizzoni, D. M. Menge, G. Zhou, D. Zhong, A. M. Vardo-Zalik, A. K. Githeko, and G. Yan (2009). High prevalence of asymptomatic plasmodium falciparum infections in a highland area of western Kenya: a cohort study. *Journal of Infectious Diseases* 200(1), 66–74. 10
- Baton, L. and L. Ranford-Cartwright (2005). Spreading the seeds of million-murdering death: metamorphoses of malaria in the mosquito. *Trends Parasitol.* 21(12), 573–80. 3, 4, 22
- Beck-Johnson, L., W. Nelson, K. Paaijmans, A. Read, M. Thomas, and O. Bjørnstad (2013). The effect of temperature on anopheles mosquito population dynamics and the potential for malaria transmission. *PLoS ONE 8*(11), e79276. 3
- Buchwald, A. G., J. E. Coalson, L. M. Cohee, J. A. Walldorf, N. Chimbiya, A. Bauleni, K. Nkanaunena, A. Ngwira, J. D. Sorkin, D. P. Mathanga, T. E. Taylor, and M. K. Laufer (2017). Insecticide-treated net effectiveness at preventing plasmodium falciparum infection varies by age and season. *Malaria Journal 16*(1), 32. 11
- Bushman, M., R. Antia, V. Udhayakumar, and J. C. de Roode (2018, 08). Within-host competition can delay evolution of drug resistance in malaria. *PLOS Biology 16*(8), 1–25. 23
- CDC (2020). Malaria About Malaria: Where Malaria Occurs. https://www.cdc.gov/malaria/about/distribution.html. Accessed 12/27/2021. 22
- Chitnis, N., J. M. Hyman, and J. M. Cushing (2008). Determining important parameters in the spread of malaria through the sensitivity analysis of a mathematical model. *Bull. Math. Biol.* 70, 1272–1296. 10
- Coalson, J. E., J. A. Walldorf, L. M. Cohee, M. D. Ismail, D. Mathanga, R. J. Cordy, M. Marti, T. E. Taylor, K. B. Seydel, M. K. Laufer, and M. L. Wilson (2016). High prevalence of plasmodium falciparum gametocyte infections in school-age children using molecular detection: patterns and predictors of risk from a cross-sectional study in southern Malawi. *Malaria Journal* 15(1), 527. 5, 11, 16, 23
- Dawes, E., T. Churcher, S. Zhuang, R. Sinden, and M. Basáñez (2009). Anopheles mortality is both age- and Plasmodium-density dependent: implications for malaria transmission. *Malar J.* 12(8), 228. 4
- Desai, M., A. M. Buff, S. Khagayi, P. Byass, N. Amek, A. van Eijk, L. Slutsker, J. Vulule, F. O. Odhiambo, P. A. Phillips-Howard, et al. (2014). Age-specific malaria mortality rates in the KEMRI/CDC health and demographic surveillance system in Western Kenya, 2003–2010. *PloS one 9*(9), e106197. 10
- Eikenberry, S. and A. Gumel (2018). Mathematical modeling of climate change and malaria transmission dynamics: a historical review. *J. Math. Biol. 77*, 857–933. 5
- Filipe, J., E. Riley, C. Drakeley, C. Sutherland, and A. Ghani (2007). Determination of the processes driving the acquisition of immunity to malaria using a mathematical transmission model. *PLoS computational biology 3*(12), e255. 10



- Garba, S. and U. Danbaba (2020). Modeling the effect of temperature variability on malaria control strategies. *Math. Model. Nat. Phenom.* 15, 65. 4, 5
- Johnson, L. W. and R. D. Riess (1982). Numerical Analysis. Addison-Wesley. 3
- Kariuki, S. M., K. Rockett, T. G. Clark, H. Reyburn, T. E. Agbenyega, T.and Taylor, G. L. Birbeck, T. N. Williams, and C. R. Newton (2013). The genetic risk of acute seizures in African children with falciparum malaria. *Epilepsia 54*(6), 990–1001. 11, 16, 23
- Kavwenje, S., L. Zhao, L. Chen, and E. Chaima (2022). Projected temperature and precipitation changes using the lars-wg statistical downscaling model in the shire river basin, malawi. *International Journal of Climatology* 42(1), 400–415. 5
- Kindong, R., J. Chen, L. Dai, C. Gao, D. Han, S. Tian, J. Wu, Q. Ma, and J. Tang (2021). The effect of environmental conditions on seasonal and inter-annual abundance of two species in the Yangtze river estuary. *Marine and Freshwater Research* 72, 493–506. 5
- Kweka, E., G. Zhou, T. Gilbreath III, Y. Afrane, A. Nyindo, M. and Githeko, and G. Yan (2011). Predation efficiency of anopheles gambiae larvae by aquatic predators in Western Kenya highlands. *Parasites and Vectors* 4(128). 15
- Makanga, M. and S. Krudsood (2009). The clinical efficacy of artemether/lumefantrine (coartem®). *Malaria Journal 8*(1), S1–S8. 23
- Manore, C., M. Teboh-Ewungkem, O. Prosper, A. Peace, K. Gurski, and Z. Feng (2019). Intermittent preventive treatment (IPT): Its role in averting disease-induced mortality in children and in promoting the spread of antimalarial drug resistance. *Bull. Math. Biol.* 81(1), 193–234. 3, 6, 10, 22
- Mathanga, D., E. Walker, M. Wilson, D. Ali, T. Taylor, and M. Laufer (2012). Malaria control in Malawi: Current status and directions for the future. *Acta Trop 121*(3), 212–217. 11, 16
- Miazgowicz, K., M. Shocket, S. Ryan, O. Villena, R. Hall, J. Owen, T. Adanlawo, K. Balaji, L. Johnson, E. Mordecai, et al. (2020). Age influences the thermal suitability of *plasmodium falciparum* transmission in the Asian malaria vector *anopheles stephensi*. *Proceedings of the Royal Society B 287* (1931), 20201093. 11, 12
- Mitchell, C. and C. Kribs (2017). A comparison of methods for calculating the basic reproductive number for periodic epidemic systems. *Bull. Math. Biol.* 79, 1846–1869. 15
- Mitchell, C. and C. Kribs (2019). Invasion reproductive numbers for periodic epidemic systems. *Infectious Disease Modelling 4*, 124–141. 15
- Mordecai, E., J. Caldwell, M. Grossman, C. Lippi, L. Johnson, M. Neira, J. Rohr, S. Ryan, V. Savage, M. Shocket, R. Sippy, A. Stewart Ibarra, M. Thomas, and O. Villena (2019). Thermal biology of mosquito-borne disease. *Ecol Lett.* 10, 1690–1708.
- Mordecai, E. A., K. P. Paaijmans, L. R. Johnson, C. Balzer, T. Ben-Horin, E. de Moor, A. McNally, S. Pawar, S. J. Ryan, T. C. Smith, and K. D. Lafferty (2013). Optimal temperature for malaria transmission is dramatically lower than previously predicted. *Ecology Letters* 16(1), 22–30. 4, 11, 12
- Mzilahowa, T., I. Hastings, M. Molyneux, and et al. (2012). Entomological indices of malaria transmission in Chikhwawa district, Southern Malawi. *Malar J 11*, 380. 11, 16
- National Malaria Control Programme, Ministry of Health & Population, L. (2010). National malaria control programme: Malawi malaria program performance review. Accessed: 05/13/2022. 13
- Ngwa, G., M. Teboh-Ewungkem, Y. Dumont, R. Ouifki, and J. Banasiak (2019). On a three-stage structured model for the dynamics of malaria transmission with human treatment, adult vector demographics and one aquatic stage. *J Theor Biol. 481*, 202–222. 3
- Okuneye, K. and A. Gumel (2017). Analysis of a temperature- and rainfall-dependent model for malaria transmission dynamics. *Math Biosci.* 287, 72–92. 4, 5
- O'Meara, W., D. Smith, and F. McKenzie (2006). Potential impact of intermittent preventive treatment (IPT) on spread of drug resistant malaria. *PLoS Medicine* 3(5), 633–642. 10



- Pascual, M., J. A. Ahumada, L. F. Chaves, X. Rodo, and M. Bouma (2006). Malaria resurgence in the east African highlands: temperature trends revisited. *Proceedings of the National Academy of Sciences 103*(15), 5829–5834. 4, 5
- Pathak, A. K., J. C. Shiau, M. B. Thomas, and C. C. Murdock (2019). Field relevant variation in ambient temperature modifies density-dependent establishment of Plasmodium falciparum gametocytes in mosquitoes. *Frontiers in Microbiology 10*, 2651. 3, 4
- Plowe, C. V. (2022). Malaria chemoprevention and drug resistance: a review of the literature and policy implications. *Malaria Journal 21*(1), 1–25. 5
- Posny, D. and J. Wang (2014). Computing the basic reproductive numbers for epidemiological models in nonhomogeneous environments. *Applied Mathematics and Computation* 242, 473–490. 15, 16
- Roth, S., M. Teboh-Ewungkem, and M. Li (2019). Predicting suitability of regions for Zika outbreaks with zero-inflated models trained using climate data. 22
- Roux, O. and V. Robert (2019). Larval predation in malaria vectors and its potential implication in malaria transmission: an overlooked ecosystem service? *Parasites Vectors 12*(217). 15
- Shapiro, L., S. Whitehead, and M. Thomas (2017). Quantifying the effects of temperature on mosquito and parasite traits that determine the transmission potential of human malaria. *PLOS Biology 15*(10), e2003489. 22
- Sippy, R., D. Herrera, D. Gaus, R. E. Gangnon, J. A. Patz, and J. E. Osorio (2019, 05). Seasonal patterns of dengue fever in rural Ecuador: 2009-2016. *PLOS Neglected Tropical Diseases* 13(5). 5
- Slater, H. C., B. D. Foy, K. Kobylinski, C. Chaccour, O. J. Watson, J. Hellewell, G. Aljayyoussi, T. Bousema, J. Burrows, U. D'Alessandro, H. Alout, F. O. Ter Kuile, P. G. T. Walker, A. C. Ghani, and M. R. Smit (2020). Ivermectin as a novel complementary malaria control tool to reduce incidence and prevalence: a modelling study. *The Lancet Infectious Diseases* 20(4), 498–508.
- Stoer, J. and R. Bulirsch (1980). Introduction to Numerical Analysis. New York: Springer-Verlag. 13
- Suh, E., M. Grossman, J. Waite, N. Dennington, E. Sherrard-Smith, T. Churcher, and M. Thomas (2020). The influence of feeding behaviour and temperature on the capacity of mosquitoes to transmit malaria. *Nature Ecology and Evolution 4*, 940–951. 3, 4
- Talisuna, A. O., P. E. Okello, A. Erhart, M. Coosemans, and U. D'Alessandro (2007). Intensity of malaria transmission and the spread of Plasmodium falciparum–resistant malaria: a review of epidemiologic field evidence. *The American journal of tropical medicine and hygiene 77*(6 Suppl), 170–180. 23
- Teboh-Ewungkem, M., J. Mohammed-Awel, F. F.N. Baliraine, and S. Duke-Sylvester (2014). The effect of intermittent preventive treatment on anti-malarial drug resistance spread in areas with population movement. *Malaria Journal 13*, 428. 3, 6, 10
- Teboh-Ewungkem, M., C. Podder, and A. Gumel (2010). Mathematical Study of the Role of Gametocytes and an Imperfect Vaccine on Malaria Transmission Dynamics. *Bull. Math. Biol. 72*(1), 63–93. 4
- Teboh-Ewungkem, M. and T. Yuster (2010). A within-vector mathematical model of Plasmodium falciparum and implications of incomplete fertilization on optimal gametocyte sex ratio. *J Theor Biol* 264, 273–86. 4
- Teboh-Ewungkem, M. I. and G. A. Ngwa (2020). Fighting malaria with ivermectin: a novel malaria control tool. *The Lancet Infectious Diseases 20*(4), 394–395. 3
- Teboh-Ewungkem, M. I. and G. A. Ngwa (2021). Covid-19 in malaria-endemic regions: potential consequences for malaria intervention coverage, morbidity, and mortality. *The Lancet Infectious Diseases 21*(1), 5–6. 3
- Teboh-Ewungkem, M. I., O. Prosper, K. Gurski, C. A. Manore, A. Peace, and Z. Feng (2015). Intermittent Preventive Treatment (IPT) and the Spread of Drug Resistant Malaria. In *Applications of Dynamical Systems in Biology and Medicine*, pp. 197–233. Springer. 3, 6, 7, 10, 22
- Thieme, H. (2009). Spectral bound and reproduction number for infinite dimensional population structure and time heterogeneity. SIAM J Appl Math 70, 188–211. 15



- van den Driessche, P. and J. Watmough (2002). Reproduction numbers and sub-threshold endemic equilibria for compartmental models of disease transmission. *Mathematical Biosciences 180*(1), 29–48. 15
- Wang, W. and X.-Q. Zhao (2008). Threshold dynamics for compartmental epidemic models in periodic environments. *J Dyn Diff Equat 20*, 699–717. 15
- Warnatzsch, E. A. and D. S. Reay (2019). Temperature and precipitation change in malawi: Evaluation of cordex-africa climate simulations for climate change impact assessments and adaptation planning. *Science of the Total Environment 654*, 378–392.
- Weather Climate Online (2021). Chikwakwa Climate Weather Averages. Accessed 12/27/2021. 22
- Weiss, D., A. Bertozzi-Villa, S. Rumisha, P. Amratia, R. Arambepola, K. Battle, E. Cameron, E. Chestnutt, H. Gibson, J. Harris, S. Keddie, J. Millar, J. Rozier, T. Symons, C. Vargas-Ruiz, S. Hay, D. Smith, P. Pedro L Alonso, A. Noor, S. Bhatt, and P. Gething (2020). Indirect effects of the COVID-19 pandemic on malaria intervention coverage, morbidity, and mortality in Africa: a geospatial modelling analysis. *Lancet Infect Dis. 21*, P59–69. 3
- WHO (2018). Malaria, Malawi profile. https://www.who.int/malaria/publications/country-profiles/profile\_mwi\_en.pdf?ua=1. Accessed 7/22/2020. 11
- WHO (2021a). Malaria. https://www.who.int/news-room/fact-sheets/detail/malaria. Accessed 12/20/2021. 3,22
- WHO (2021b). Zeroing in on malaria elimination: final report of the E-2020 initiative. https://apps.who.int/iris/handle/10665/340881. 3
- World Bank Group (2019). Climate Change Knowledge Portal: For Development Practitioners and Policy Makers Country Malawi. https://climateknowledgeportal.worldbank.org/country/malawi/climate-data-historical. Accessed: 01/06/2020. 12, 14, 16, 17, 18, 22